2009

Traffic-adaptive, flow-specific medium access for wireless networks

Walker, T. Owens

Monterey, California. Naval Postgraduate School

NAVAL
POSTGRADUATE
SCHOOL

TECHNICAL REPORT

NPS-EC-09-002

Traffic-adaptive, Flow-specific Medium Access for Wireless Networks

by

T. Owens Walker III, Murali Tummala, and John McEachen

12 August 2009

Approved for public release; distribution is unlimited

Prepared for: U.S. Special Operations Command
MacDill AFB, FL

THIS PAGE INTENTIONALLY LEFT BLANK

NAVAL POSTGRADUATE SCHOOL
Monterey, California 93943-5000

Daniel T. Oliver, VADM, USN (Ret)
President

Leonard A. Ferrari
Provost

This report was prepared for U.S. Special Operations Command
and funded by Space and Naval Warfare Systems Center Atlantic.

This report was prepared by:

CDR T. Owens Walker III, USN
PhD Student, Department of Electrical and Computer Engineering

Murali Tummala
Professor, Department of Electrical and Computer Engineering

John McEachen
Professor, Department of Electrical and Computer Engineering

Reviewed by:

Jeffrey B. Knorr
Department of Electrical and Computer Engineering

Released by:

Karl A. van Bibber
Vice President and
Dean of Research

THIS PAGE INTENTIONALLY LEFT BLANK

REPORT DOCUMENTATION PAGE			Form Approved OMB No. 0704-0188
Public reporting burden for this collection of information is estimated to average 1 hour per response, including the time for reviewing instruction, searching existing data sources, gathering and maintaining the data needed, and completing and reviewing the collection of information. Send comments regarding this burden estimate or any other aspect of this collection of information, including suggestions for reducing this burden, to Washington headquarters Services, Directorate for Information Operations and Reports, 1215 Jefferson Davis Highway, Suite 1204, Arlington, VA 22202-4302, and to the Office of Management and Budget, Paperwork Reduction Project (0704-0188) Washington DC 20503.			
1. AGENCY USE ONLY ***(Leave blank)***	**2. REPORT DATE** August 2009	**3. REPORT TYPE AND DATES COVERED** Technical Report	
4. TITLE AND SUBTITLE: Title (Mix case letters) Traffic-adaptive, Flow-specific Medium Access for Wireless Networks			**5. FUNDING NUMBERS**
6. AUTHOR(S) T. Owens Walker III, Murali Tummala, and John McEachen			
7. PERFORMING ORGANIZATION NAME(S) AND ADDRESS(ES) Naval Postgraduate School Monterey, CA 93943-5000			**8. PERFORMING ORGANIZATION REPORT NUMBER**
9. SPONSORING /MONITORING AGENCY NAME(S) AND ADDRESS(ES) N/A			**10. SPONSORING/MONITORING AGENCY REPORT NUMBER**
11. SUPPLEMENTARY NOTES The views expressed in this report are those of the author and do not reflect the official policy or position of the Department of Defense or the U.S. Government.			
12a. DISTRIBUTION / AVAILABILITY STATEMENT Distribution Statement (mix case letters)			**12b. DISTRIBUTION CODE**

13. ABSTRACT (maximum 200 words)

In this report, we formally introduce the novel concept of traffic-adaptive, flow-specific medium access control and show that it outperforms contention, non-contention and hybrid medium access schemes. A traffic-adaptive, flow-specific mechanism is proposed that utilizes flow-specific queue size statistics to select between medium access modes. A general model for traffic-adaptive, flow-specific medium access control is developed and it is shown that hybrid medium access as well as traditional contention-based and non-contention schemes can be seen as special cases of the more general flow-specific access. The two-flow, two-mode case of the general model is developed in detail and it is shown analytically that this queue-based implementation of traffic-adaptive, flow-specific medium access outperforms contention, non-contention, and hybrid approaches. The proposed traffic-adaptive, flow-specific mechanism is applied to Cooperative Wireless Sensor Network Medium Access Control (CWS-MAC) a flow-specific medium access protocol. Performance is evaluated is evaluated and compared to the traditional medium access approaches. Both analytical and simulation results are provided including the development of throughput and delay expressions for slotted ALOHA with periodic server vacations.

14. SUBJECT TERMS Flow-specific; Traffic-adaptive; Cross layer; Medium access control; Wireless sensor network			**15. NUMBER OF PAGES** 86
			16. PRICE CODE
17. SECURITY CLASSIFICATION OF REPORT Unclassified	**18. SECURITY CLASSIFICATION OF THIS PAGE** Unclassified	**19. SECURITY CLASSIFICATION OF ABSTRACT** Unclassified	**20. LIMITATION OF ABSTRACT** UU

NSN 7540-01-280-5500 Standard Form 298 (Rev. 2-89)
Prescribed by ANSI Std. 239-18

THIS PAGE INTENTIONALLY LEFT BLANK

ABSTRACT

In this report, we formally introduce the novel concept of traffic-adaptive, flow-specific medium access control and show that it outperforms contention, non-contention and hybrid medium access schemes. A traffic-adaptive, flow-specific mechanism is proposed that utilizes flow-specific queue size statistics to select between medium access modes. A general model for traffic-adaptive, flow-specific medium access control is developed and it is shown that hybrid medium access as well as traditional contention-based and non-contention schemes can be seen as special cases of the more general flow-specific access. The two-flow, two-mode case of the general model is developed in detail and it is shown analytically that this queue-based implementation of traffic-adaptive, flow-specific medium access outperforms contention, non-contention, and hybrid approaches. The proposed traffic-adaptive, flow-specific mechanism is applied to Cooperative Wireless Sensor Network Medium Access Control (CWS-MAC) a flow-specific medium access protocol. Performance is evaluated is evaluated and compared to the traditional medium access approaches. Both analytical and simulation results are provided including the development of throughput and delay expressions for slotted ALOHA with periodic server vacations.

THIS PAGE INTENTIONALLY LEFT BLANK

TABLE OF CONTENTS

THIS PAGE INTENTIONALLY LEFT BLANK

LIST OF FIGURES

THIS PAGE INTENTIONALLY LEFT BLANK

I. INTRODUCTION

Wireless medium access solutions generally fall into two categories: contention-based and scheduled (contention-free). It has been well established that the collision-free approach of scheduled schemes, such as [1], provide high throughput in high demand scenarios at the expense of overhead and packet delay. In comparison, contention-based approaches, such as [2], [3], provide low delay times at low to moderate network loads, but performance begins to degrade rapidly as the network becomes saturated.

Initial work has been done in the wireless sensor network field to combine the benefits of both approaches in response to changing network load. Most notably, [4] provides a contention-based approach that utilizes TDMA framing to provide "hints" for contention resolution. In these types of approaches, though, medium access is tailored to overall network conditions, not to the characteristics of the individual flows.

In [5], we proposed a solution that has the capability to provide medium access on a *per flow* basis. Designed to support both low demand, delay sensitive control traffic and high demand, delay tolerant data traffic, Cooperative Wireless Sensor Medium Access Control (CWS-MAC) is a distributed, flow-specific medium access scheme. However, to fully realize the potential performance gains, a flow-specific scheme must be responsive to changes in traffic characteristics within each flow. Accordingly, the primary objective of this work is to present an adaptive medium access solution that can not only accommodate multiple flows with different traffic characteristics, but also respond to traffic changes *within a given flow*.

The contribution of this paper is three-fold. First, traffic-adaptive, flow-specific medium access control is formally defined and shown to provide better performance than contention-based, non-contention-based and hybrid medium access schemes. Second, a general model for a traffic-adaptive, flow-specific medium access control is presented. The two-flow, two-mode case is developed in detail and contention-based, contention-free as well as hybrid approaches are shown to be special cases of this general flow-specific model. Third, a queue-based, traffic-adaptive, flow-specific medium access

control mechanism is proposed and applied to CWS-MAC to provide relevant performance analysis and simulation results.

The organization of this report is as follows. Chapter II formally introduces the concept of traffic-adaptive, flow-specific medium access and demonstrates its performance advantage over existing approaches. In Chapter III, a queue-based, traffic-adaptive, flow-specific mechanism is proposed and a general model for a traffic-adaptive, flow-specific medium access control is developed. Chapter IV applies this proposed mechanism to the CWS-MAC protocol and provides accompanying performance analysis. Simulation results are included in Chapter V.

II. TRAFFIC-ADAPTIVE, FLOW-SPECIFIC MEDIUM ACCESS

To provide motivation for traffic-adaptive, flow-specific medium access, we begin with an examination of the delay performance of various contention-based and non-contention-based medium access schemes. The mean packet delay for Aloha [2], slotted Aloha [6], several CSMA variants [3], and TDMA [7] is plotted in Figure 1 as a function of the normalized load. This normalized load is equivalent to the steady state throughput and is normalized by the channel rate. For the purposes of the plot, channel rate is 1 Mbps, packet size is 1000 bits, there are 100 slots in a TDMA frame (each slot is one packet length in duration) and $a = 0.01$ for the CSMA schemes. The CSMA plots represent the best case achievable delay at steady state. For these delay curves, we assume Poisson arrivals and the appropriate delay equations can be found in [2], [6], [3], [7].

It can be seen that at low loads, the delay performance of the contention schemes is better, while at higher loads, the delay performance of the non-contention scheme is

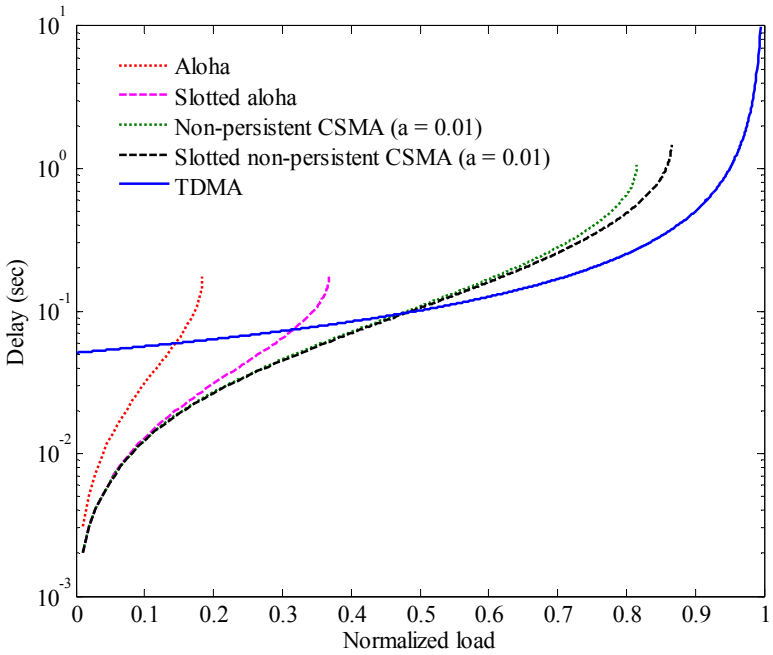

Figure 1. Packet delay plotted as a function of normalized load for TDMA and CSMA. Channel rate is 1 Mbps, packet size is 1000 bits, and there are 100 slots (one packet length in duration) in the TDMA frame.

better. It is natural then to ask if we can get the delay performance of CSMA at low loads and that of TDMA at high loads. This is precisely the strategy of hybrid approaches such as [4],[8] which treat the flows in aggregate and transition from a contention-based approach to a non-contention-based approach as the load increases. In an aggregate flow that is comprised of both low and high demand flows, these hybrid schemes have the disadvantage of increased delay for flows that could take advantage of the lower delays associated with the contention-based approaches. In contrast, we propose to treat each flow individually to optimize both the overall performance and the performance on a per flow basis.

We now formally define the terms flow-specific medium access and traffic-adaptive, flow-specific medium access and provide an example to illustrate the concept.

Definition: Flow-specific medium access control is a medium access approach that provides medium access on a per flow basis. It is capable of concurrently providing different medium access schemes to different traffic flows.

Definition: Traffic-adaptive, flow-specific medium access control is a flow-specific medium access approach that is capable of dynamically switching between multiple medium access schemes to respond to traffic variations within a given flow.

As an illustrative example, we examine an aggregate flow that is comprised of two individual packet flows. We assume that the load of the first flow is low while the load of the second flow varies from low to high. The aggregate flow demand, then, will vary with the second flow. This example models the behavior of an event-based wireless sensor network that includes both a control flow to provide sensor coordination within the network and a data flow that corresponds to sensor data transmission to a designated sink such as that shown in Figure 2. Prior to event detection, the demand of both flows is low (perhaps in a periodic reporting state). Upon event detection, the control flow remains relatively low demand (control packets are small in size and are only needed

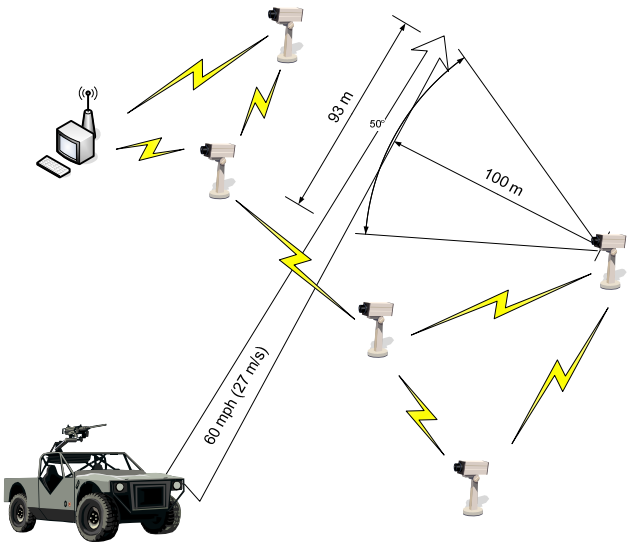

Figure 2. Battlefield example of a wireless sensor network. The data traffic from the video cameras to the command and control point (sink) and the control traffic required to manipulate the camera (focus, azimuth, elevation, etc.) form two distinct traffic flows.

periodically to update sensor parameters) while the data flow will increase dramatically as recorded event data is forwarded to the sink.

In this example, contention-based [2],[3] and non-contention-based [7] schemes will treat the flows in aggregate and provide either contention-based or non-contention-based access to the combined flow. A traffic-adaptive, hybrid scheme [4],[8] will again treat the flows together, but will transition from contention-based to non-contention-based medium access when the demand of the aggregate flow reaches some threshold. In contrast, a traffic-adaptive, flow-specific approach will treat the two flows individually by continuing to provide contention-based medium access to the low demand control flow while the data flow is transitioned from contention-based to non-contention-based access as its load increases.

Defining the aggregate delay performance as the weighted sum of the delay performance for the individual flows, we can evaluate and compare the delay performance of the different approaches for this two-flow example [3],[4],[7]. In Figure 3, we plot the mean aggregate packet delay as a function of aggregate load for the four approaches. The normalized load of the first flow is fixed at 0.1 while the load of the second flow is allowed to vary from 0.0 to 0.8. We can clearly see that while the hybrid approach takes advantage of the lower delays of CSMA in the low contention region and

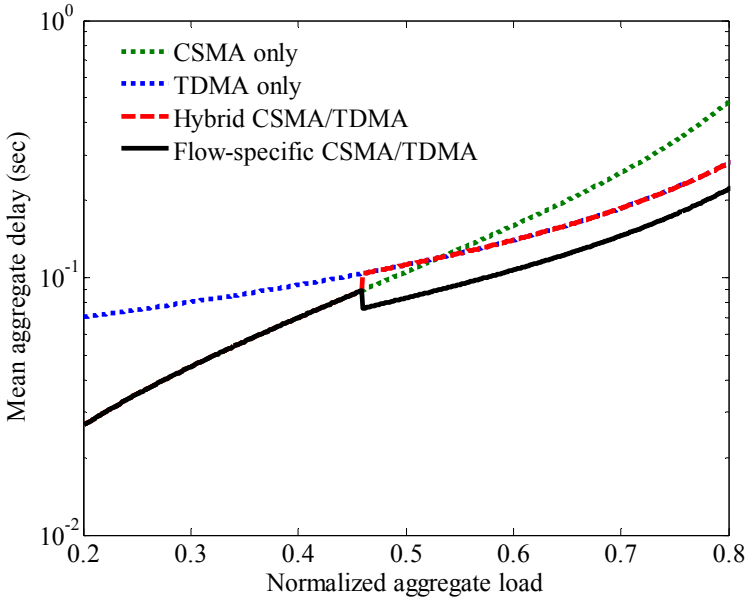

Figure 3. Packet delay plotted as a function of normalized load for slotted nonpersistent CSMA [3], TDMA [7], hybrid and flow-specific medium access (using CSMA/TDMA). Channel rate is 1 Mbps, packet size is 1000 bits, there are 100 slots in a TDMA frame (each slot is one packet length in duration) and $a = 0.01$ for the CSMA schemes. The CSMA plot assumes steady state and represents minimum achievable delay.

TDMA in the high contention region, the traffic-adaptive, flow-specific approach offers better overall delay performance in the high contention region by allowing the low demand control flow to remain in the contention-based mode.

Figure 3 illustrates the advantage of a traffic-adaptive, flow-specific approach in this particular example. In the following theorem and associated corollary, we extend this to the general case and show that the traffic-adaptive, flow-specific approach outperforms contention, non-contention and aggregate hybrid medium access schemes provided that the per flow switchover point between the access modes is chosen correctly.

Theorem: Given a suitable switching point is chosen at which a flow will transition between medium access schemes, flow-specific medium access will provide as good or better delay performance than contention, non-contention, and hybrid medium access schemes.

Proof: First, let us consider the case of the contention-based medium access scheme. Without a loss of generality, we will assume that the mean packet delays D_i for the N individual flows i are ordered as in $D_1 \le D_2 \le \cdots \le D_m \le \cdots \le D_{N-1} \le D_N$. The switching point between access schemes is then chosen such that

$$\begin{aligned} D_i^c &\le D_i^{nc} \quad \text{for all } i = 1:m \\ D_i^c &> D_i^{nc} \quad \text{for all } i = (m+1):N \end{aligned} \tag{1}$$

where D_i^c is the contention-based access scheme delay for flow i and D_i^{nc} is the non-contention-based access scheme delay for flow i. The mean aggregate delay for the flow-specific access scheme is

$$D_{flow} = \sum_{i=1}^{N} \left(\frac{\lambda_i}{\lambda} \right) D_i \tag{2}$$

where λ_i is the arrival rate for flow i and the aggregate arrival rate λ is the sum of the individual flow arrival rates. From (1), the mean overall delay of (2) is equivalent to

$$D_{flow} = \sum_{i=1}^{m} \left(\frac{\lambda_i}{\lambda} \right) D_i^c + \sum_{i=m+1}^{N} \left(\frac{\lambda_i}{\lambda} \right) D_i^{nc}. \tag{3}$$

Using proof by contradiction, suppose that the contention-based medium access provides lower aggregate mean delay than the flow-specific scheme or $D_{flow} > D_{cont}$. Expanding these,

$$\sum_{i=1}^{m} \left(\frac{\lambda_i}{\lambda} \right) D_i^c + \sum_{i=m+1}^{N} \left(\frac{\lambda_i}{\lambda} \right) D_i^{nc} > \sum_{i=1}^{N} \left(\frac{\lambda_i}{\lambda} \right) D_i^c \tag{4}$$

Breaking apart the contention-based term on the right side of the inequality, we have

$$\begin{aligned} &\sum_{i=1}^{m} \left(\frac{\lambda_i}{\lambda} \right) D_i^c + \sum_{i=m+1}^{N} \left(\frac{\lambda_i}{\lambda} \right) D_i^{nc} \\ &\qquad > \sum_{i=1}^{m} \left(\frac{\lambda_i}{\lambda} \right) D_i^c + \sum_{i=m+1}^{N} \left(\frac{\lambda_i}{\lambda} \right) D_i^c \end{aligned} \tag{5}$$

which can then be reduced to

$$\sum_{i=m+1}^{N} \left(\frac{\lambda_i}{\lambda} \right) D_i^{nc} > \sum_{i=m+1}^{N} \left(\frac{\lambda_i}{\lambda} \right) D_i^c \tag{6}$$

This implies that

$$D_i^c < D_i^{nc} \quad \text{for some } i = (m+1):N \tag{7}$$

which contradicts (1). Thus, $D_{flow} \leq D_{cont}$ and flow-specific medium access will provide as good or better delay performance than a contention-based scheme. The non-contention case is proven in a similar manner. Finally, the hybrid scheme can be considered as the either a contention scheme when the aggregate load is below the switching point or a non-contention scheme when it is above. Accordingly, it can be broken into two cases and is proved in a similar manner as well. *Q.E.D.*

Corollary: Given a suitable switching point is chosen at which a flow will transition between medium access schemes and that there exist at least two flows which are in two different medium access modes, flow-specific medium access will provide better delay performance than contention, non-contention, and hybrid medium access schemes.

Proof: This corollary follows directly from the theorem since it can be shown that the equality in performance only occurs when m is either 1 or N. The constraint that there exists at least one flow in each of the contention and non-contention modes implies that $1 < m < N$ and, therefore, that the delay performance of the traffic-adaptive, flow-specific approach is strictly better than the other schemes.

As can be seen from this discussion, the performance of a traffic-adaptive medium access scheme is tied to the selection of the switching point [4]. Returning to our two-flow example, the impact of the selection of the switching point can be plainly seen in Figure 4 where we plot mean aggregate delay versus normalized aggregate load for four different switching points. In the next chapter, we propose a queue-based, traffic-adaptive mechanism to dynamically implement this switching point.

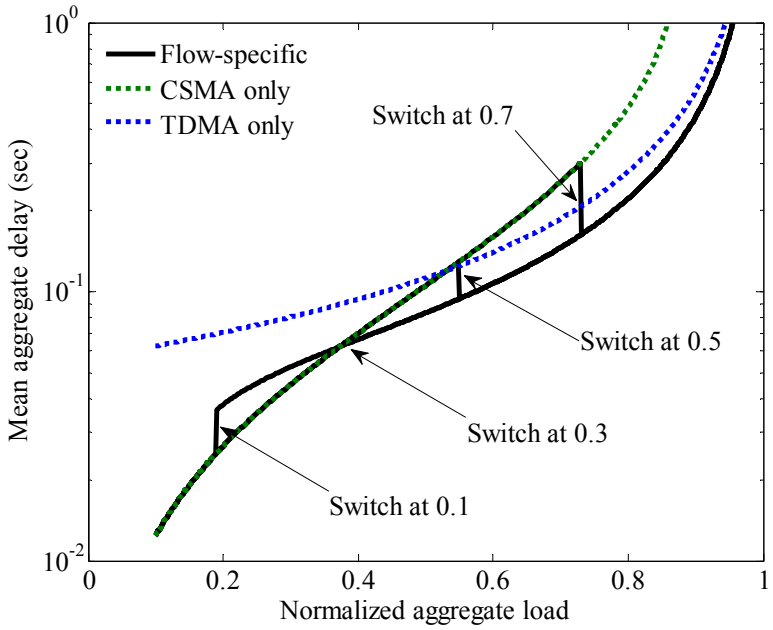

Figure 4. Flow-specific delay plotted against the normalized load and our compared to CSMA and TDMA for various switchover points. Channel rate is 1 Mbps, packet size is 1000 bits, there are 100 slots in a TDMA frame (each slot is one packet length in duration) and $a = 0.01$ for the CSMA schemes. The CSMA plot assumes steady state and represents minimum achievable delay.

THIS PAGE INTENTIONALLY LEFT BLANK

III. TRAFFIC-ADAPTIVE, FLOW-SPECIFIC MEDIUM ACCESS MECHANISM

To realize the potential performance gains identified in the previous chapter, we propose a traffic-adaptive, flow-specific mechanism in this section that utilizes flow-specific queue size statistics and develop a general traffic-adaptive, flow-specific medium access control performance model. In the final two subsections, we examine the two-flow and single-flow cases in detail and demonstrate that contention, non-contention and hybrid schemes are special cases of the general flow-specific model.

A. TRAFFIC-ADAPTIVE, FLOW-SPECIFIC MEDIUM ACCESS MECHANISM

Assuming each flow (or each set of flows if we choose to group a set of flows with similar characteristics together) has its own queue at each node, we use this queue size as an indicator of flow-specific traffic contention. Queue size has been used extensively, both implicitly and explicitly, as a measure of congestion across a network [9]. As local buffers fill up, strategies include explicit control packet information to "choke" the flow from the sender as well as different packet dropping approaches, such as [10] and its many variants, that lead to retransmissions and implicit congestion notification. The use of queue size has also begun to migrate into wireless sensor network traffic estimation. For example, although TRAMA [1] does not explicitly exchange queue sizes, it does exchange schedules that signal the presence of packets in the local buffers. As an alternate to queue size, network load in the form of contention can be estimated directly by measuring the loss rate associated with acknowledgement packets or indirectly by measuring the channel noise level [4]. The drawback of these approaches to traffic estimation is that they are not flow-specific and therefore do not facilitate flow-specific medium access decisions.

The proposed queue-based traffic-adaptive, flow-specific medium access mechanism operates as follows. As flow load reaches a predetermined threshold, measured in terms of the flow-specific queue size, the flow is switched from one access mode to another. Each flow (or each set of flows) will have its own queue and associated thresholds. These thresholds, $\theta_{1,f,m}$ and $\theta_{2,f,m}$, define the switching point discussed in the previous section and can be unique for each flow f and medium access mode m as shown in Figure 5. The single-flow, two-mode (contention and non-contention) case is illustrated in Figure 6. When the queue size reaches $\theta_{1,f}$, flow f is switched from

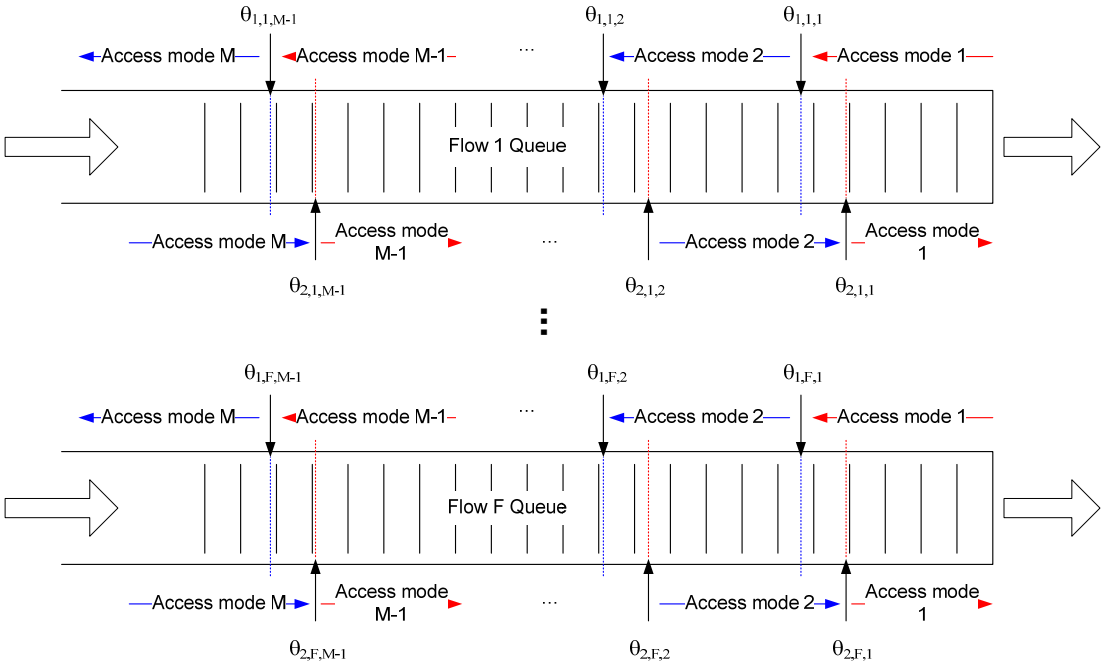

Figure 5. Flow-specific queues and associated thresholds for general traffic-adaptive, flow-specific medium access model.

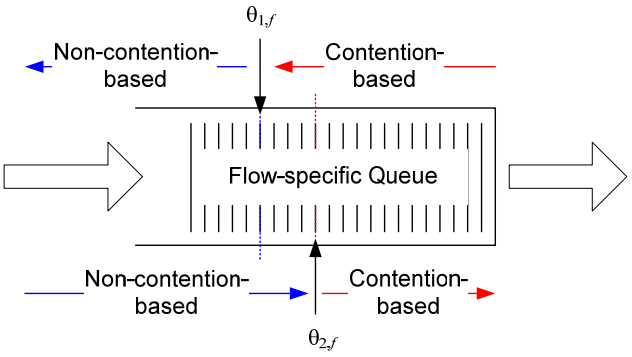

Figure 6. Single-flow, two-mode version of the proposed traffic-adaptive, flow-specific mechanism.

contention-based to non-contention-based medium access. Similarly, when the queue size drops to $\theta_{2,f}$, the flow is switched from non-contention-based back to contention-based medium access. In the next section, we develop a general model that provides insight into the choice of these thresholds.

B. A GENERAL PERFORMANCE MODEL FOR TRAFFIC-ADAPTIVE, FLOW-SPECIFIC MEDIUM ACCESS

Traffic-adaptive, flow-specific medium access can be modeled as a finite state machine as shown in Figure 7. Each state is uniquely specified by a vector that reflects the access mode of each flow. The number of states required, Φ, is, therefore, a function of the number of flows, *F*, and the number of unique medium access modes, *M*, as $\Phi = (M)^F$. If we assume that the underlying, individual queues are M/M/1, then this finite-state model can be viewed as a hidden Markov model [11]. To determine the steady state probabilities π_s associated with the individual observable states *s*, we must first derive the state probabilities of the hidden Markov model and then establish the relationships between these Markov states and the observable states. In the special case where $\theta_{1,f,m} = \theta_{2,f,m}$ (i.e., a system with no hysteresis), each probability π_s is a function of a unique, non-overlapping set of the underlying Markov state probabilities. With these

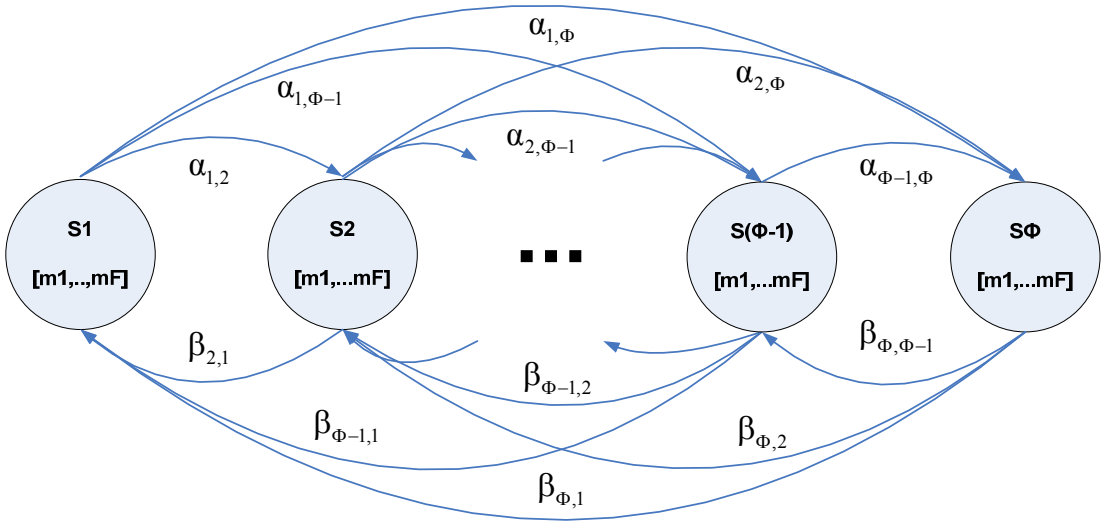

Figure 7. General traffic-adaptive, flow-specific finite state model.

steady state probabilities, the mean throughput S and delay D for the flow-specific medium access scheme can then be developed as

$$S = \sum_{s=1}^{\Phi} \pi_s S_s \text{ and } D = \sum_{s=1}^{\Phi} \pi_s D_s \tag{8}$$

where S_s and D_s are the mean throughput and delay, respectively, experienced in state s.

In general, the medium access scheme for flow f will transition from one access mode m_i to the next mode m_{i+1} when the number of packets in the flow-specific queue reaches the threshold θ_{1,f,m_i} denoted by $\alpha_{s,s+1}$ in Figure 7. Similarly, the transition from $s+1$ to s occurs when the number of packets drops to $\theta_{2,f,m}$ denoted by $\beta_{s+1,s}$. The probability of these transitions is a function of both the number of packets N_f in the flow-specific queue f and the utilization in the current observed state. The utilization $\rho_{m,s,f}$ is defined as the ratio of the packet arrival rate for flow f to the service time for flow f and is unique to the state s and the flow f. Given the result for a M/M/1 queue that the total number of customers N in the system is [15]

$$N = \frac{\rho}{1-\rho}, \tag{9}$$

the utilization can be derived from Little's Law [15] as

$$\rho_{s,f} = \frac{\lambda_f D_s}{1+\lambda_f D_s} \tag{10}$$

where λ_f is the packet arrival rate for flow f and D_s is the mean delay in state s. In the following section, we will examine this relationship closer for the two-flow, two-mode case and develop both throughput and delay expressions for the example of Chapter II.

C. TWO-FLOW, TWO-MODE (CONTENTION, NON-CONTENTION) CASE

As shown in Figure 8, it requires a four-state model to represent a two-flow, flow-specific medium access scheme such as one capable of providing both contention and non-contention access modes. We can make a set of simplifying assumptions to allow us to compare the performance of this traffic-adaptive mechanism to that of the ideal case in the example of Chapter II. Without a loss of generality, we assume that it is flow 1 that

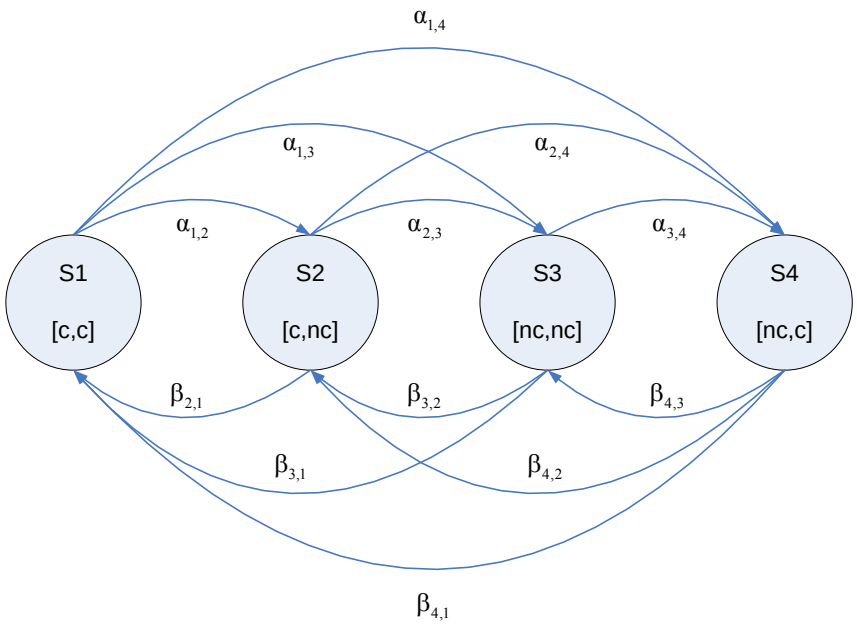

Figure 8. Full 4-state model for two-flow flow-specific, medium access.

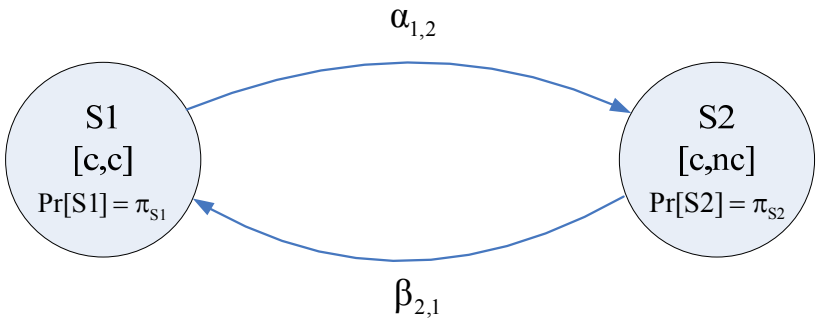

Figure 9. Simplified 2-state model for two-flow flow-specific, medium access.

has a constant arrival rate and remains in the contention-based access mode while flow 2 is allowed to transition between access modes as its arrival rate varies. Accordingly, $\alpha_{1,2}$ and $\beta_{2,1}$ are the only non-zero transition rates since states S3 and S4 are not achievable and the full model of Figure 8 can be reduced to the two-state model of Figure 9.

Assuming that the underlying Markov process is M/M/1, the bilevel hysteretic service rate control work of [12] can be adopted to arrive at the steady state probabilities by viewing the system as having two distinct service rates μ_1 and μ_2 (corresponding to the states S1 and S2). The states of this underlying Markov Chain are defined by the state the system is in (S1 or S2 from Figure 9) and the queue size (number of packets awaiting transmission). The transition from μ_1 to μ_2 occurs when the number of packets in the

queue of flow 2 reaches $\theta_{1,2}$ and the transition from μ_2 to μ_1 occurs when the number of packets in the queue of flow 2 drops to $\theta_{2,2}$ as shown in Figure 6. Examining the underlying Markov model, shown in Figure 10, the state probabilities P_n (where *n* is the queue length) are given by [12]

$$
\begin{aligned}
P_n &= \left(\rho_{1,2}\right)^n P_0 && n \subset \left[0, \theta_{2,2} - 1\right] \\
P_{\theta_{2,2}+i} &= \frac{\left(\rho_{1,2}\right)^{\theta_{1,2}-1} \rho_{2,2} \left(1-\rho_{1,2}\right)\left(\left(\rho_{1,2}\right)^i - \left(\rho_{1,2}\right)^\Delta\right)\left(1-\left(\rho_{2,2}\right)^i\right)}{\left(1-\left(\rho_{1,2}\right)^\Delta\right)\left(1-\rho_{1,2}\right)\left(1-\rho_{2,2}\right)} P_0 && i \subset \left[0, \Delta - 1\right] \qquad (11) \\
P_{\theta_{1,2}+j-1} &= \frac{\left(\rho_{1,2}\right)^{\theta_{1,2}-1}\left(1-\rho_{1,2}\right)\left(1-\left(\rho_{2,2}\right)^\Delta\right)}{\left(1-\left(\rho_{1,2}\right)^\Delta\right)\left(1-\rho_{2,2}\right)} \left(\rho_{2,2}\right)^j P_0 && j \subset \left[1, \infty\right]
\end{aligned}
$$

where

$$
P_0 = \left(\frac{1}{\left(1-\rho_{1,2}\right)} - \frac{\Delta\left(\rho_{1,2}\right)^{\theta_{1,2}-1}\left(\rho_{1,2}-\rho_{2,2}\right)}{\left(1-\left(\rho_{1,2}\right)^\Delta\right)\left(1-\rho_{2,2}\right)} \right)^{-1} \qquad (12)
$$

and $\Delta = \theta_{1,2} - \theta_{2,2}$ captures the extent of the hysteresis loop created by $\theta_{1,2}$ and $\theta_{2,2}$. Returning to our two-state medium access model of Figure 9, the probability that the system is in state S2, π_{S2}, is equivalent to the probability that the system is in service rate μ_2 which can be shown to be [12]

$$
\pi_{S2} = \frac{\Delta\left(\rho_{1,2}\right)^{\theta_{1,2}-1}\left(\rho_{2,2}\right)\left(1-\rho_{1,2}\right)}{\left(1-\left(\rho_{1,2}\right)^\Delta\right)\left(1-\rho_{2,2}\right)} P_0 . \qquad (13)
$$

The probability that the system is in state S1 is then simply $\pi_{S1} = 1 - \pi_{S2}$. The steady state probabilities are plotted as a function of $\theta_{1,2}$ in Figure 11. It can be seen that, as expected, for the limiting cases of $\theta_{1,2}$ approaching zero and $\theta_{1,2}$ approaching infinity, the probability that the flow-specific medium access scheme is in State 2 approaches one ($\pi_{S2} = 1$) and zero ($\pi_{S2} = 0$), respectively.

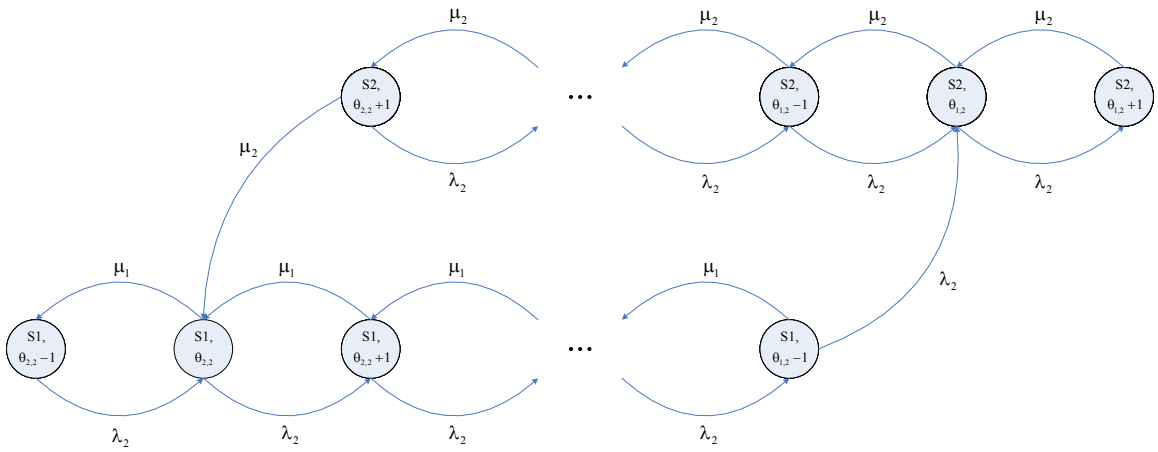

Figure 10. Underlying Markov Chain for two-flow, two-mode example.

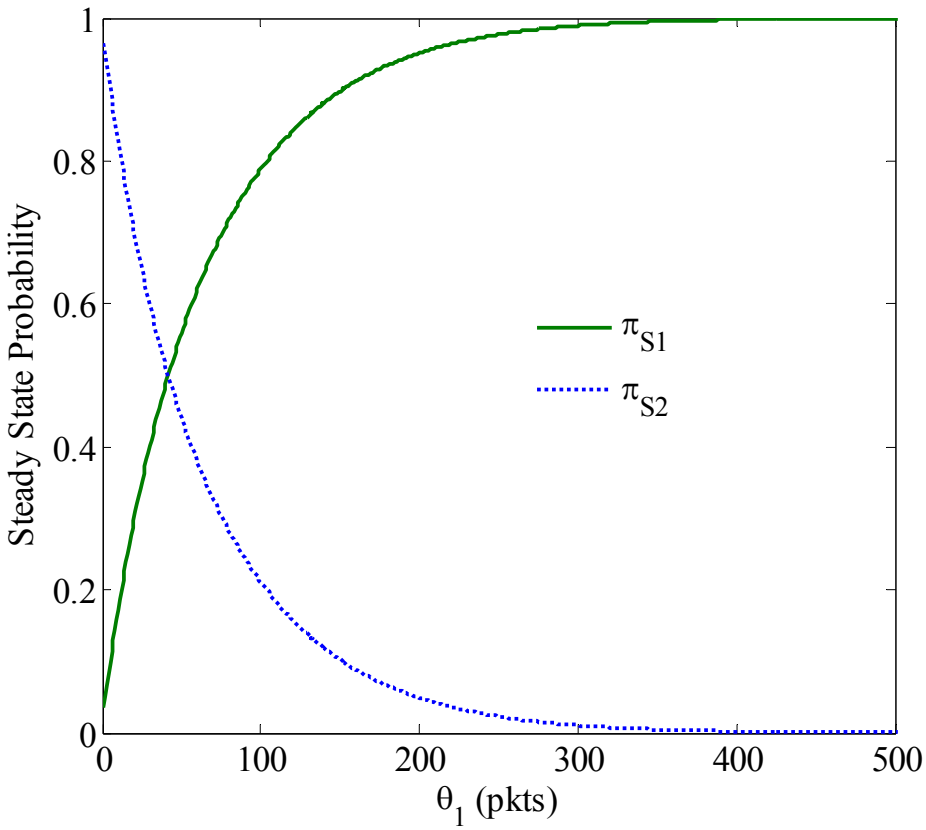

Figure 11. Steady state probability for two-flow, two-mode model as a function of the queue-based threshold, θ_1.

Following the analysis of Chapter II, the associated state throughputs and delays are

$$S_{S1} = S^c \text{ and } S_{S2} = \frac{\lambda_1}{\lambda} S_1^c + \frac{\lambda_2}{\lambda} S_2^{nc}$$
$$D_{S1} = D^c \text{ and } D_{S2} = \frac{\lambda_1}{\lambda} D_1^c + \frac{\lambda_2}{\lambda} D_2^{nc} \tag{14}$$

where S^c and D^c are the throughput and delay, respectively, of the aggregate flow in the contention mode, S_f^c and D_f^c are the throughput and delay, respectively, of flow *f* in the contention mode, and S_f^{nc} and D_f^{nc} are the throughput and delay, respectively, of flow *f* in the non-contention mode. Substituting (13) and (14) into (8), we can then develop the resulting aggregate mean throughput and delay expressions as

$$S = S^c + \frac{\Delta\left(\rho_{1,2}\right)^{\theta_{1,2}-1}\left(\rho_{2,2}\right)\left(1-\rho_{1,2}\right)}{\left(1-\left(\rho_{1,2}\right)^{\Delta}\right)\left(1-\rho_{2,2}\right)} P_0\left(\frac{\lambda_1}{\lambda} S_1^c + \frac{\lambda_2}{\lambda} S_2^{nc} - S^c\right)$$
$$D = D^c + \frac{\Delta\left(\rho_{1,2}\right)^{\theta_{1,2}-1}\left(\rho_{2,2}\right)\left(1-\rho_{1,2}\right)}{\left(1-\left(\rho_{1,2}\right)^{\Delta}\right)\left(1-\rho_{2,2}\right)} P_0\left(\frac{\lambda_1}{\lambda} D_1^c + \frac{\lambda_2}{\lambda} D_2^{nc} - D^c\right). \tag{15}$$

This analysis of the special case where the demand of one flow is fixed can be extended to the two-flow, *M*-mode case with $M > 2$ using the more general variable service rate work of [13].

Using the parameters of the example in Chapter II, we plot mean aggregate delay as a function of normalized load in Figure 12 for $\theta_1 = 20$ and $\theta_2 = 5$. It can be seen that, as expected, the flow-specific scheme performs as well as CSMA when the aggregate load is low and outperforms all three approaches when a flow exists in both the contention and non-contention modes. The role of θ_1 as the switching point can be clearly seen in Figure 13 where we plot both delay and throughput as a function of load for various values of θ_1. At the optimum value for θ_1 (close to 20 packets in this example), the mechanism transitions to contention-free operation as the delay curves intersect. At values below optimum, the scheme transitions too early and the aggregate delay at low loads suffers. For values of θ_1 above optimum, the scheme transitions late and the heavy load begins to overwhelm the contention-based mode, the delay grows and the throughput saturates (and will eventually drop off).

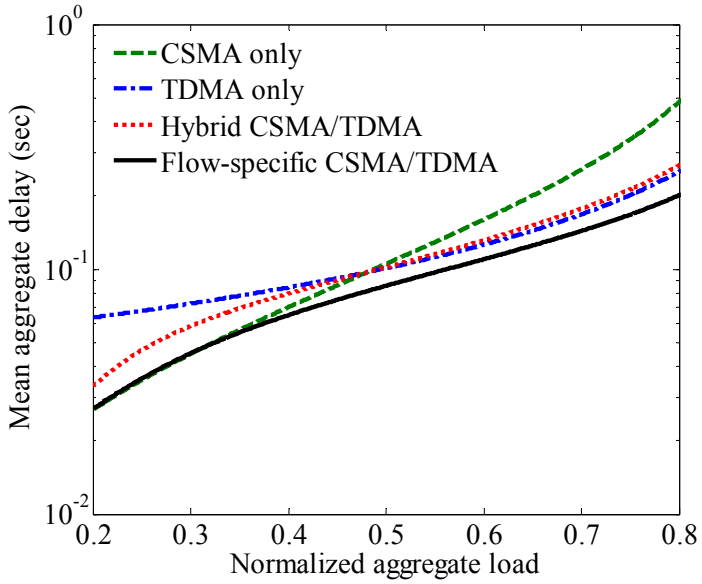

Figure 12. Packet delay plotted as a function of normalized load for slotted nonpersistent CSMA, TDMA, hybrid using CSMA/TDMA and flow-specific medium access using CSMA/TDMA with $\theta_1 = 20$ and $\theta_2 = 5$. Channel rate is 1 Mbps, packet size is 1000 bits, there are 100 slots in a TDMA frame (each slot is one packet length in duration) and $a = 0.01$ for the CSMA schemes. The CSMA plot assumes steady state and represents minimum achievable delay.

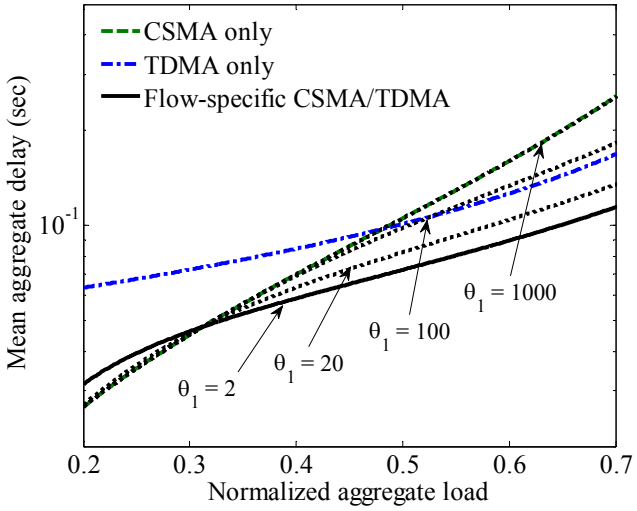

(a)

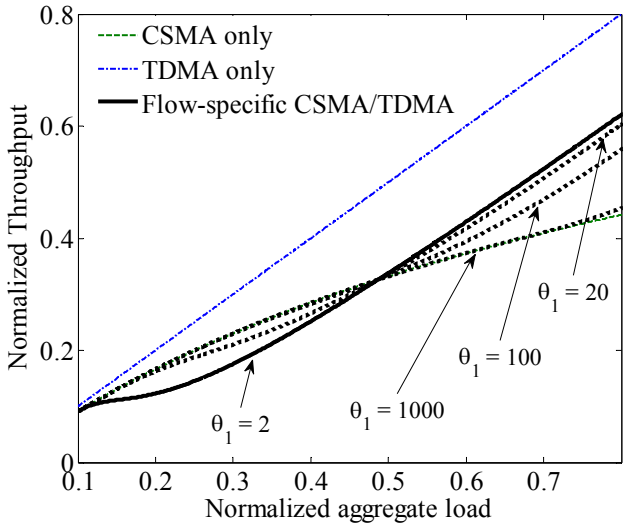

(b)

Figure 13. Mean aggregate (a) delay and (b) throughput plotted as a function of the normalized aggregate load for multiple values of θ_1. Channel rate is 1 Mbps, packet size is 1000 bits, there are 100 slots in a TDMA frame (each slot is one packet length in duration) and $a = 0.01$ for the CSMA schemes. The CSMA plot assumes steady state and represents minimum achievable delay.

D. SINGLE-FLOW, TWO-MODE CASE: HYBRID MEDIUM ACCESS

The model of Figure 9 can be further simplified if we examine the single-flow case. This case can be shown to be equivalent to the hybrid case where multiple flows are treated in aggregation. Thus, hybrid approaches represent a special case of the more general flow-specific approach. To demonstrate this, we note that there is a single, aggregate queue in a hybrid scheme, so $\theta_{1,2}$ and $\theta_{2,2}$ reduce to θ_1 and θ_2, respectively, and $\rho_{1,2}$ and $\rho_{2,2}$ reduce to $\rho_1 = \rho_c$ and $\rho_2 = \rho_{nc}$, respectively. Following the analysis of the previous section, the state probabilities are

$$\begin{aligned} \pi_{nc} &= \frac{\Delta(\rho_c)^{\theta_1 - 1}(\rho_{nc})(1-\rho_c)}{\left(1-(\rho_c)^{\Delta}\right)(1-\rho_{nc})} P_0 \\ \pi_c &= 1 - \pi_{nc} \end{aligned} \tag{16}$$

where

$$P_0 = \left(\frac{1}{(1-\rho_c)} - \frac{\Delta(\rho_c)^{\theta_1 - 1}(\rho_c - \rho_{nc})}{\left(1-(\rho_c)^{\Delta}\right)(1-\rho_{nc})} \right)^{-1} \tag{17}$$

and $\Delta = \theta_1 - \theta_2$.

Since S_1 and S_2 are equivalent to S^c and S^{nc}, respectively, and D_1 and D_2 are equivalent to D^c and D^{nc}, respectively, the overall mean throughput is $S = \pi_c S^c + \pi_{nc} S^{nc}$ and the mean delay is $D = \pi_c D^c + \pi_{nc} D^{nc}$. Substituting (16) into these expressions, we arrive at

$$\begin{aligned} S &= S^c + \frac{\Delta(\rho_c)^{\theta_1 - 1}(\rho_{nc})(1-\rho_c)}{\left(1-(\rho_c)^{\Delta}\right)(1-\rho_{nc})} P_0 \left(S^{nc} - S^c\right) \\ D &= D^c + \frac{\Delta(\rho_c)^{\theta_1 - 1}(\rho_{nc})(1-\rho_c)}{\left(1-(\rho_c)^{\Delta}\right)(1-\rho_{nc})} P_0 \left(D^{nc} - D^c\right). \end{aligned} \tag{18}$$

This result is included in Figure 12 for $\theta_1 = 20$ and $\theta_2 = 5$.

E. SINGLE-FLOW, SINGLE-MODE CASE

Finally, it is straightforward to show that the contention only [2],[3] and non-contention [7] schemes are trivial single-flow, single-mode cases of the general flow-specific model. The state probabilities for the contention-based scheme are $\pi_{S1} = \pi_c = 1$ and $\pi_{S2} = \pi_{nc} = 0$ while they are $\pi_{S1} = \pi_c = 0$ and $\pi_{S2} = \pi_{nc} = 1$ for the non-contention-based scheme. Substituting these into (8), we arrive $S = S^c$ and $D = D^c$ for the contention-based scheme and $S = S^{nc}$ and $D = D^{nc}$ for the non-contention-based scheme.

IV. TRAFFIC ADAPTIVE CWS-MAC

We now apply this proposed flow-specific, traffic-adaptive mechanism to the Cooperative Wireless Sensor Network Medium Access Control (CWS-MAC) protocol, a distributed, flow-specific medium access scheme. We begin with an overview of CWS-MAC and then discuss the application of the proposed mechanism. We include performance analysis using the general model developed in the previous chapter.

A. OVERVIEW OF CWS-MAC

CWS-MAC [5] is a fixed, flow-specific medium access control that is designed to accommodate multiple flows based on flow demand. Application-aware, it combines the low demand delay performance of a contention-based scheme with the high demand throughput performance of a non-contention (scheduled) approach. In [5], we refer to the "control" and "data" flows. In this report, we generalize these and their respective medium access mechanisms to "contention-based" and "non-contention-based."

The underlying non-contention-based medium access mechanism is provided by a TDMA scheme in which nodes are assigned slots within the TDMA frame for transmission of their non-contention flow packets. Slot assignment can be accomplished through a dynamic, distributed scheduling algorithm such as [16], [17], [18].

The contention-based medium access mechanism is superimposed on top of the TDMA framing through the use of an interframe space and a contention beacon that effectively give the contention-based flow global (across node) priority over the non-contention-based flow. A node with contention flow packets to transmit signals its intent to seize the current TDMA slot by transmitting a contention beacon of length, t_b. Although not specifically addressed in [5], in a multi-hop network this beacon must be retransmitted to all two-hop neighbors of the originating node. A node with non-contention packets to transmit must wait for the duration of the interframe space, t_{IFS}, and then sense the medium. If the medium is free (i.e., no contention beacon has been transmitted in its two-hop neighborhood), the packet may transmit its non-contention packets. If a beacon is detected, the slot owner defers and the slot is effectively seized as a contention slot. To ensure the non-contention flow is not "choked off," a portion of the

original TDMA slot is set aside in the contention slot for use by the slot owner for non-contention packet transmission.

To reduce collisions among competing nodes with contention-based traffic to transmit within the two-hop neighborhood, the contention slot is subdivided into a series of transmission minislots. A version of slotted ALOHA [6], a node will transmit in a minislot with some predetermined probability (calculated as the inverse of the number of minislots in [5]) and an acknowledgement mechanism is included to recover from collisions.

An illustration of the CWS-MAC frame is provided in Figure 14. User selectable parameters for CWS-MAC include the slot size, t_s, the minislot size, t_{ms}, the number of minislots, k, and the lengths of the control beacon and interframe space. A strategy is provided in [5] to select these parameters to optimize throughput and delay performance.

B. TRAFFIC-ADAPTIVE CWS-MAC

CWS-MAC gains its performance improvement by handling application flows differently based on their traffic characteristics. As implemented in [5], though, medium access modes are statically assigned to each flow and CWS-MAC has no capability to adapt to changes in traffic flow demand over time. To fully realize the potential performance gains of CWS-MAC, the hybrid control must be aware of and respond to changes in flow traffic characteristics. We therefore apply the queue-based, flow-specific,

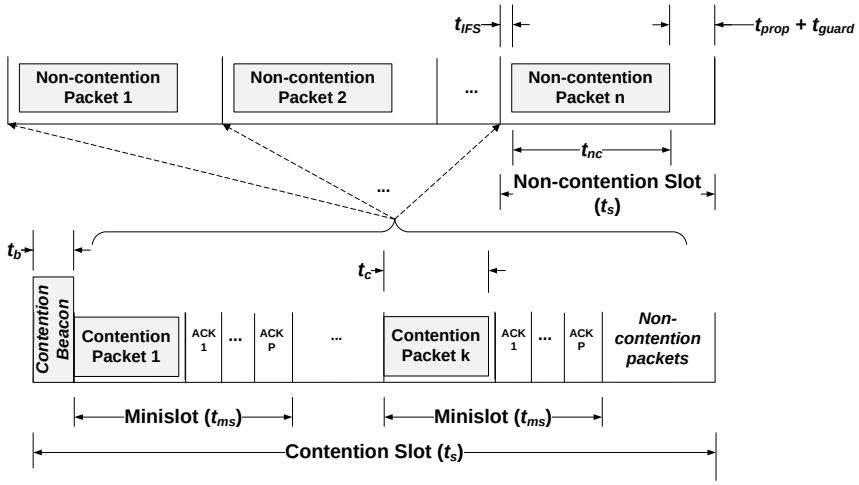

Figure 14. An illustration of the CWS-MAC mechanism and frames.

traffic-adaptive mechanism of Chapter III to CWS-MAC.

The flow-specific queues are maintained at the link layer which implies that the link layer mechanism is capable of determining which flow a packet is associated with. The queue size measurement is taken whenever a packet is added or removed from the applicable queue. It should be noted that while a non-contention mode packet is removed from the queue upon transmission, a contention mode packet is not removed until the appropriate acknowledgement is received at the sender. Although certainly not required, this queue size measurement can be smoothed by applying a moving average to it. When a flow is transitioned from one mode to another, all queued packets within that flow are transitioned as well. This has the effect of "clearing" out the flow from the prior access mode and specifically improves delay and throughput recovery time when a flow is transitioned from the contention mode to the non-contention mode.

The distributed nature of traffic-adaptive CWS-MAC leads to a subtle point that should not be overlooked: neighboring nodes may assign the same flow to different medium access modes. This is because the state transitions of Figure 8 are based on local queue statistics which will vary between neighboring nodes. This does not pose a problem in traffic-adaptive CWS-MAC because the medium access mode is specific to the sender not the receiver and a receiver needs no prior arrangement to receive a flow in a given mode. Hence, although a node may receive a flow in one mode, it requires no coordination to switch to reception in the other mode and it is free to retransmit the flow in either mode.

C. PERFORMANCE ANALYSIS OF TRAFFIC-ADAPTIVE CWS-MAC

In this section, we develop individual expressions for the non-contention and contention throughput and delay for traffic-adaptive CWS-MAC. We then combine these using (15) to arrive at the overall mean delay and throughput for the example of Chapter II.

1. Non-contention throughput for CWS-MAC

We begin with the non-contention throughput. At steady state, the arrival rate is equivalent to the departure rate and the normalized non-contention throughput, S^{nc}, is given by [19]

$$S^{nc} = \frac{\Lambda_{nc}\bar{L}_{nc}}{R} \tag{19}$$

where Λ_{nc} is the mean total arrival rate for the non-contention mode, $\bar{L}_{nc}$ is the mean packet size (in bits) for the non-contention mode, and *R* is the channel rate in bps. For a TDMA-based scheme, this throughput is bounded by a maximum value that is dependent on the per frame overhead. Specifically,

$$S^{nc}_{\max} = \frac{M\bar{T}_{data}}{t_f} \tag{20}$$

where $\bar{T}_{data}$ is the mean time spent in a slot transmitting useful data, t_f is the frame length in seconds and we have assumed, without loss of generality, that each node is assigned a single slot in the frame. Clearly, $M\bar{T}_{data} = t_f - \bar{T}_{ovrhd}$ where $\bar{T}_{ovrhd}$ is the mean time spent in a frame on overhead and (20) can alternately be written as

$$S^{nc}_{\max} = 1 - \frac{\bar{T}_{ovrhd}}{t_f}. \tag{21}$$

To calculate $\bar{T}_{data}$, we must account for both the non-contention and contention slots in Figure 14. In the first case, T_{data} for a packet transmitted in a non-contention slot is equal to t_{nc}. This value is reduced in the case of the contention slot by the overhead associated with the contention access mode which can be seen in Figure 14 to be $t_b + kt_{ms}$. Combining these cases (and accounting for the t_{IFS} term), we have

$$T_{data} = \begin{cases} t_{nc} & \text{for a non-contention slot} \\ t_{nc} + t_{IFS} - t_b - kt_{ms} & \text{for a contention slot} \end{cases} \tag{22}$$

for *k* minislots per slot and

$$t_{nc} = t_s - t_{IFS} - t_{prop} - t_{guard}. \tag{23}$$

We can calculate $\bar{T}_{data}$ then as

$$\begin{aligned} \bar{T}_{data} = {} & T_{data}[\text{non-contention slot}] \times \Pr[\text{non-contention slot}] \\ & + T_{data}[\text{contention slot}] \times \Pr[\text{contention slot}] \end{aligned} \tag{24}$$

which, from (22), can be written as

$$\begin{aligned} \bar{T}_{data} = {} & t_{nc} \Pr[\text{non-contention slot}] \\ & + \left(t_{nc} + t_{IFS} - t_b - kt_{ms}\right) \Pr[\text{contention slot}]. \end{aligned} \tag{25}$$

Assuming that the contention mode arrivals follow a Poisson distribution, the probabilities in (25) can be derived as follows. The probability that a slot is designated as a non-contention slot is equivalent to the probability that there are no control packet arrivals during the previous slot and that no control packet retransmissions are pending from the previous contention slot. For now, we will assume that the probability of the latter is negligible (we will come back to this point in a follow-on section). Focusing then on the first term,

Pr[non-contention slot] = Pr[no contention packets arrivals in previous slot] (26)

Since the contention packet arrivals are Poisson, this can be shown to be

$$\Pr[\text{non-contention slot}] \equiv p_0 = e^{-\Lambda_c t_s} \tag{27}$$

where the aggregate control mode packet arrival rate $\Lambda_c = M\lambda_c$ for M nodes. The Pr[contention slot] is simply $1 - \Pr[\text{non-contention slot}]$ or

$$\Pr[\text{contention slot}] = 1 - p_0 = 1 - e^{-\Lambda_c t_s}. \tag{28}$$

Substituting (27) and (28) into (25), we have

$$\overline{T}_{data} = t_{nc} e^{-\Lambda_c t_s} + \left(t_{nc} + t_{IFS} - t_b - kt_{ms}\right)\left(1 - e^{-\Lambda_c t_s}\right). \tag{29}$$

Rearranging terms,

$$\overline{T}_{data} = t_{nc} + \left(1 - e^{-\Lambda_c t_s}\right)\left(t_{IFS} - t_b - kt_{ms}\right), \tag{30}$$

and substituting into (20)

$$S_{\max}^{nc} = \frac{M\left(t_{nc} + \left(1 - e^{-\Lambda_c t_s}\right)\left(t_{IFS} - t_b - kt_{ms}\right)\right)}{t_f}. \tag{31}$$

Recognizing that $t_s = \frac{t_f}{M}$, we finally arrive at

$$S_{\max}^{nc} = \frac{t_{nc} + \left(1 - e^{-\Lambda_c t_s}\right)\left(t_{IFS} - t_b - kt_{ms}\right)}{t_s}. \tag{32}$$

Combining (32) and (19), we can express the throughput for the non-contention mode as

$$S^{nc} = \begin{cases} \dfrac{\Lambda_{nc}\overline{L}}{R} & \Lambda_{nc} \le S_{\max}^{nc}\left(\dfrac{R}{\overline{L}}\right) \\ S_{\max}^{nc} & \text{otherwise} \end{cases}. \tag{33}$$

The capture the effect of the ratio of T_{data} for the contention slot to that for a non-contention slot or, equivalently, the percentage of the bandwidth allocated to the contention flow, we define β as

$$\beta = \frac{t_b + kt_{ms}}{t_s}. \tag{34}$$

Thus, $\beta \in [0,1]$ and, if the timing parameters in (34) are fixed, is proportional to the choice of k. A larger value of β represents a larger percentage of bandwidth allocated to the contention mode. A plot of maximum non-contention throughput as a function of the probability of a non-contention slot p_0 (which, as we shall see later, is a function of the aggregate contention packet arrival rate) for various values of β is provided in Figure 15.

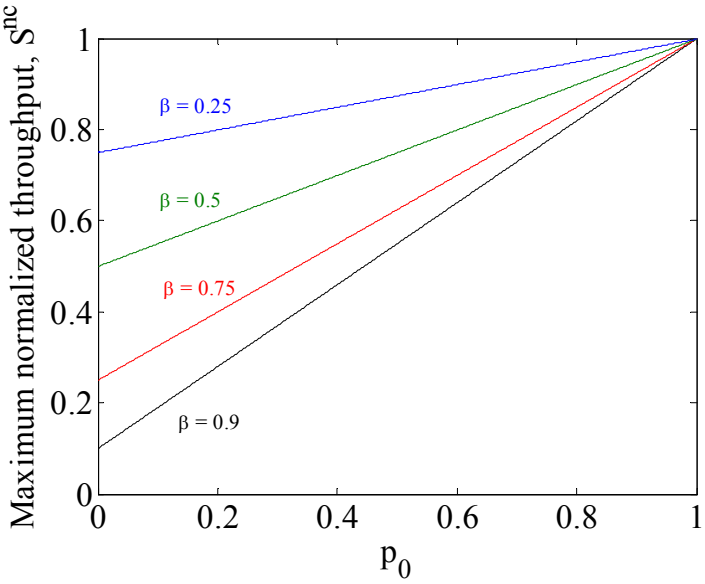

Figure 15. Maximum non-contention throughput as a function of a function of the probability of a non-contention slot p_0 for various values of β.

2. Non-contention mean delay for CWS-MAC

Turning our attention to latency, the mean delay of a packet in the non-contention mode is comprised of four parts [19]: (1) $\overline{T}_{sync}^{nc}$, the mean delay associated with waiting for the next slot boundary (sometimes referred to as the synchronization delay); (2) $\overline{T}_{w}^{nc}$, the mean waiting time in the queue, (3) $\overline{T}_{xmt}^{nc}$, the mean transmission time and (4) t_{prop}, the maximum propagation time of the packet. This is summarized as

$$\bar{D}^{nc} = \bar{T}^{nc}_{sync} + \bar{T}^{nc}_{w} + \bar{T}^{nc}_{xmt} + t_{prop} . \tag{35}$$

To develop expressions for the first three terms, we must examine the two cases identified in the previous section. The first term, $\bar{T}^{nc}_{sync}$, is the same in both cases. Since the non-contention packet arrivals are assumed to be purely random (Poisson distributed) and the period of arrival is the slot duration t_s, then the synchronization delay is simply

$$\bar{T}^{nc}_{sync} = \frac{t_s}{2} . \tag{36}$$

To calculate the mean waiting time in the queue, $\bar{T}^{nc}_{w}$, we again assume Poisson arrivals and can therefore view the network as a set of identical M/G/1 queues where the mean arrival rate is λ_{nc}. To develop the effective service time distribution, we begin by calculating the effective service time $T^{nc}_{s_1}$ for a packet that is transmitted in a single non-contention slot. Without a loss of generality, we will assume that exactly one non-contention packet is transmitted during a non-contention slot and that each node (i.e., queue) is assigned a single slot in each frame. Thus, in this case, each queue services one packet in a frame and the effective service time is simply the frame time as in

$$T^{nc}_{s_1} = t_f . \tag{37}$$

Note that since the propagation time is specifically included in our slot time calculations (and, hence, our frame time calculations), we have implicitly included it in our effective service time.

If the first slot encountered by a packet is a contention slot, then the effective service time of a packet is increased because, as we saw in the previous section, T_{data} for a contention slot is reduced relative to that for a non-contention slot. Accordingly, the packet will be serviced over multiple slots or, equivalently, multiple frames. Let us define κ as the smallest integer, greater than or equal to the ratio of T_{data} for the non-contention slot to that for a contention slot. From (22),

$$\kappa = \left\lceil \frac{t_{nc}}{t_{nc} + t_{IFS} - t_b - kt_{ms}} \right\rceil \tag{38}$$

where $f(x) = \lceil x \rceil$ is the ceiling operator. Now, let us examine the case where a packet is serviced by a contention slot followed by a non-contention slot. In this case, the effective service time will simply be twice the frame time, t_f. Given our assumption that exactly one non-contention packet is transmitted during a non-contention slot, with some thought it can be seen that, in general, a packet service time will terminate when either the packet experiences a non-contention slot or it has spanned across κ contention slots. The service time is therefore a discrete random variable that can take on the values $\left[t_f, 2t_f, ..., (\kappa-1)t_f, \kappa t_f\right]$. By use of the ceiling operator in (38), we have made the conservative assumption that when a packet transmission spans multiple slots, any residual slot time in the last slot remains unfilled. Accordingly, our service time expression can be viewed as an upper bound which can be improved upon by allowing subsequent packets to make use this residual slot time.

We can derive the probability distribution for T_s^{nc} by examining the individual cases. The probability that a packet will encounter a single non-contention slot is simply the probability that the first slot it encounters is a non-contention slot which, from (27), is $p_0 = e^{-\Lambda_c t_s}$. The probability that T_s^{nc} will span exactly two frames is the probability of a contention slot followed by a non-contention slot or $p_0(1-p_0)$. Extending this through the case of $(\kappa-2)$ contention slots followed by a non-contention slot, we have

$$\Pr\left[T_s^{nc} = \alpha t_f\right] = p_0(1-p_0)^{\alpha-1} \qquad \text{for } 1 \le \alpha < \kappa \tag{39}$$

where α is an integer. The probability for the terminating case in which we have either $(\kappa-1)$ contention slots followed by a non-contention slot or κ consecutive contention slots is then

$$\Pr\left[T_s^{nc} = \kappa t_f\right] = 1 - \sum_{i=1}^{\kappa-1} p_0(1-p_0)^{i-1}. \tag{40}$$

Substituting $j = i-1$ and rearranging,

$$\Pr\left[T_s^{nc} = \kappa t_f\right] = 1 - p_0 \sum_{j=0}^{\kappa-2} (1-p_0)^j. \tag{41}$$

We can now use the well-known identity

$$\sum_{i=0}^{n} c^i = \frac{c^{n+1}-1}{c-1} \tag{42}$$

to simplify (41) to

$$\Pr\left[T_s^{nc} = \kappa t_f\right] = \left(1-p_0\right)^{\kappa-1}. \tag{43}$$

Combining (39) and (43) and accounting for the zero probability case of $\alpha > \kappa$, we arrive at the distribution of T_s^{nc} as

$$\Pr\left[T_s^{nc} = \alpha t_f\right] = \begin{cases} p_0\left(1-p_0\right)^{\alpha-1} & \text{for } 1 \le \alpha < \kappa \\ \left(1-p_0\right)^{\kappa-1} & \text{for } \alpha = \kappa \\ 0 & \text{for } \alpha > \kappa \end{cases}. \tag{44}$$

This result is logical when we observe that T_s^{nc} has the form of a modified geometric random variable. By this, we mean that we count the consecutive number of unsuccessful trials (contention slots, in our case) until the first successful trial (non-contention slot), but we are bounded by a maximum number of trials (κ). The probability and cumulative distribution functions for T_s^{nc} are shown in Figures 16 and 17, respectively

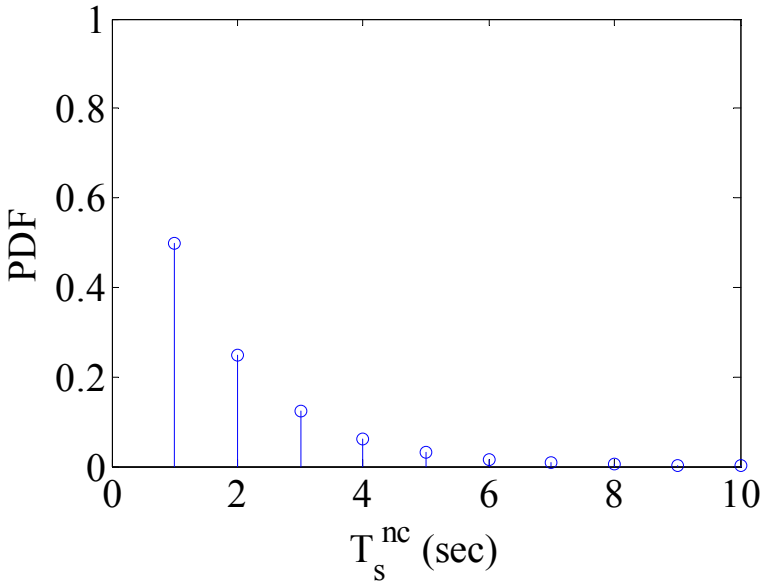

Figure 16. Probability distribution function of T_s^{nc} with $t_f = 1$ sec and $\kappa = 10$.

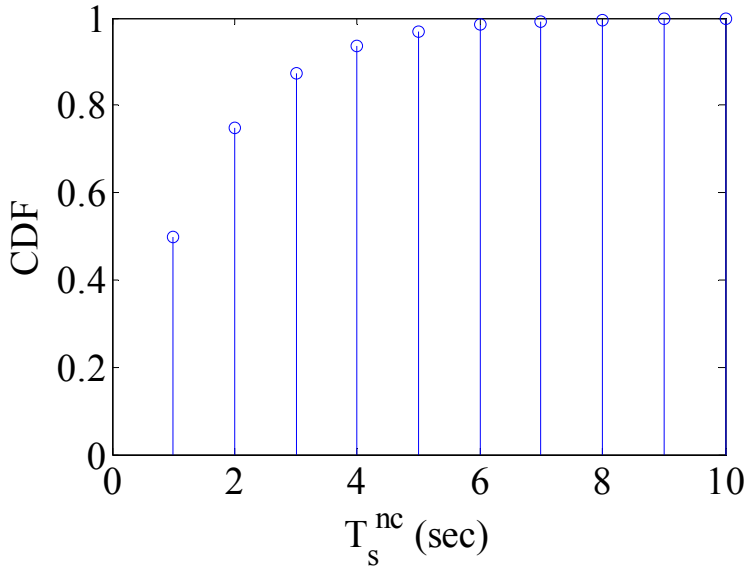

Figure 17. Cumulative distribution function of T_s^{nc} with $t_f = 1$ sec and $\kappa = 10$.

Given the distribution of T_s^{nc}, we can now calculate its mean and variance. The mean is defined as

$$E\left[T_s^{nc}\right] \equiv \bar{T}_s^{nc} = \sum_{i=1}^{\infty} T_{s_i}^{nc} \times \Pr[T_s^{nc} = T_{s_i}^{nc}]. \tag{45}$$

Making the appropriate substitutions from (44),

$$\bar{T}_s^{nc} = \sum_{i=1}^{\kappa-1} i t_f p_0 (1-p_0)^{i-1} + \kappa t_f (1-p_0)^{\kappa-1}. \tag{46}$$

Rearranging and including the case of $i = 0$ in the summation,

$$\bar{T}_s^{nc} = t_f p_0 \sum_{i=0}^{\kappa-1} i (1-p_0)^{i-1} + \kappa t_f (1-p_0)^{\kappa-1}. \tag{47}$$

To evaluate the summation in the first term, we take the partial derivative of (42)

$$\frac{\delta}{\delta c}\left(\sum_{i=0}^{n} c^i = \frac{c^{n+1}-1}{c-1}\right) \tag{48}$$

which, using the linearity property of the derivative operation, is equivalent to

$$\sum_{i=0}^{n}\left(\frac{\delta}{\delta c} c^i\right) = \frac{\delta}{\delta c}\left(\frac{c^{n+1}-1}{c-1}\right). \tag{49}$$

Evaluating this,

$$\sum_{i=0}^{n} ic^{i-1} = \frac{(n+1)c^n(c-1)-\left(c^{n+1}-1\right)}{(c-1)^2} \tag{50}$$

and making the substitutions $n = \kappa - 1$ and $c = 1 - p_0$,

$$\sum_{i=0}^{\kappa-1} i(1-p_0)^{i-1} = \frac{(\kappa-1+1)(1-p_0)^{\kappa-1}\left((1-p_0)-1\right)-\left((1-p_0)^{\kappa-1+1}-1\right)}{\left((1-p_0)-1\right)^2}. \tag{51}$$

Simplifying, we have

$$\sum_{i=0}^{\kappa-1} i(1-p_0)^{i-1} = \frac{1-(1-p_0)^{\kappa}-\kappa p_0(1-p_0)^{\kappa-1}}{{p_0}^2}. \tag{52}$$

Substituting (52) into (47),

$$\overline{T}_s^{nc} = t_f p_0\left(\frac{1-(1-p_0)^{\kappa}-\kappa p_0(1-p_0)^{\kappa-1}}{{p_0}^2}\right)+\kappa t_f(1-p_0)^{\kappa-1}. \tag{53}$$

Rearranging,

$$\overline{T}_s^{nc} = t_f\left(\frac{1-(1-p_0)^{\kappa}-\kappa p_0(1-p_0)^{\kappa-1}+\kappa p_0(1-p_0)^{\kappa-1}}{p_0}\right) \tag{54}$$

Canceling like terms, we finally arrive at the mean of T_s^{nc} as

$$\overline{T}_s^{nc} = t_f\left(\frac{1-(1-p_0)^{\kappa}}{p_0}\right) \tag{55}$$

and the square of the mean as

$$\left(\overline{T}_s^{nc}\right)^2 = \left(t_f\right)^2\left(\frac{1-(1-p_0)^{\kappa}}{p_0}\right)^2. \tag{56}$$

Checking the limiting cases of $p_0 = 1$ (all non-contention slots) and $p_0 = 0$ (all contention slots), we find that, as expected, the mean of T_s^{nc} is t_f in the former and κt_f in the latter. In the $p_0 = 0$ case, this result is arrived at through a single application of L'Hôpital's Rule. A plot of the mean of T_s^{nc} as a function of p_0 for various values of κ is provided in Figure 18.

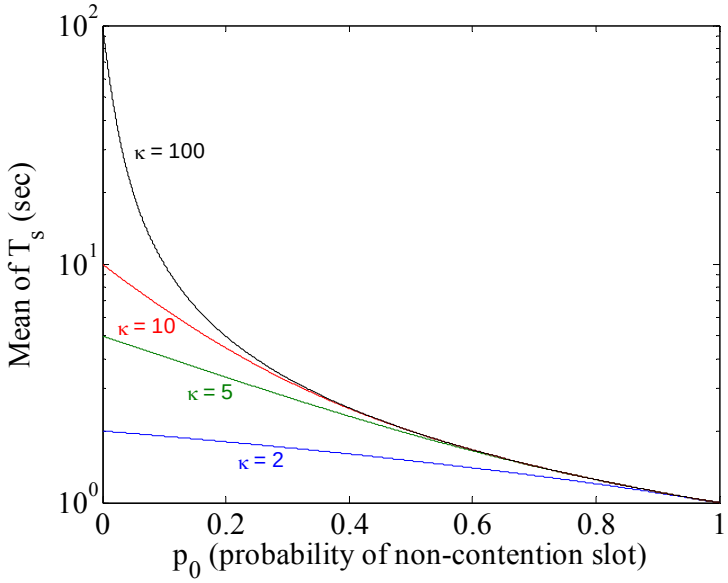

Figure 18. The mean of T_s^{nc} as a function of p_0 for various values of κ with $t_f = 1$ sec.

The second moment of the effective service time is defined as

$$E\left[\left(T_s^{nc}\right)^2\right] = \sum_{i=1}^{\infty}\left(T_{s_i}^{nc}\right)^2 \times \Pr[T_s^{nc} = T_{s_i}^{nc}] \tag{57}$$

Which, again from (44), is equivalent to

$$E\left[\left(T_s^{nc}\right)^2\right] = \sum_{i=1}^{\kappa-1}\left(it_f\right)^2 p_0\left(1-p_0\right)^{i-1} + \left(\kappa t_f\right)^2\left(1-p_0\right)^{\kappa-1} \tag{58}$$

after the appropriate substitutions. Rearranging, we have

$$E\left[\left(T_s^{nc}\right)^2\right] = \left(t_f\right)^2 p_0\sum_{i=1}^{\kappa-1} i^2\left(1-p_0\right)^{i-1} + \left(\kappa t_f\right)^2\left(1-p_0\right)^{\kappa-1}. \tag{59}$$

To evaluate the summation in the first term, we multiply (50) by c and again take the partial derivative,

$$\frac{\delta}{\delta c} c\left(\sum_{i=0}^{n} ic^{i-1} = \frac{(n+1)c^n(c-1) - \left(c^{n+1}-1\right)}{(c-1)^2}\right). \tag{60}$$

Rearranging,

$$\sum_{i=0}^{n} i\frac{\delta}{\delta c}c^i = \frac{\delta}{\delta c}\left(\frac{(n+1)c^{n+1}(c-1) - c\left(c^{n+1}-1\right)}{(c-1)^2}\right). \tag{61}$$

Differentiating the left side and multiplying out the right side,

$$\sum_{i=0}^{n} i^2 c^{i-1} = \frac{\delta}{\delta c}\left(\frac{(n+1)c^{n+2} - (n+1)c^{n+1} - c^{n+2} + c}{(c-1)^2} \right). \tag{62}$$

Combining like terms,

$$\sum_{i=0}^{n} i^2 c^{i-1} = \frac{\delta}{\delta c}\left(\frac{nc^{n+2} - (n+1)c^{n+1} + c}{(c-1)^2} \right) \tag{63}$$

and differentiating the right side,

$$\sum_{i=0}^{n} i^2 c^{i-1} = \frac{\left((n+2)nc^{n+1} - (n+1)^2 c^n + 1\right)(c-1)^2 - \left(nc^{n+2} - (n+1)c^{n+1} + c\right)2(c-1)}{(c-1)^4}. \tag{64}$$

Reducing,

$$\sum_{i=0}^{n} i^2 c^{i-1} = \frac{\left((n+2)nc^{n+1} - (n+1)^2 c^n + 1\right)(c-1) - 2\left(nc^{n+2} - (n+1)c^{n+1} + c\right)}{(c-1)^3} \tag{65}$$

and expanding the individual terms,

$$\begin{aligned} \sum_{i=0}^{n} i^2 c^{i-1} = \frac{1}{(c-1)^3}\{&\left(n^2+2n\right)c^{n+2} - \left(n^2+2n+1\right)c^{n+1} + c - \left(n^2+2n\right)c^{n+1} \\ &+ (n+1)^2 c^n - 1 - 2nc^{n+2} + 2(n+1)c^{n+1} - 2c\}. \end{aligned} \tag{66}$$

Combining terms,

$$\sum_{i=0}^{n} i^2 c^{i-1} = \frac{1}{(c-1)^3}\left\{ n^2 c^{n+2} - \left(2n^2+2n-1\right)c^{n+1} + (n+1)^2 c^n - c - 1 \right\}. \tag{67}$$

Again making the substitutions $n = \kappa - 1$ and $c = 1 - p_0$,

$$\begin{aligned} \sum_{i=0}^{\kappa-1} i^2 (1-p_0)^{i-1} = \frac{1}{(1-p_0-1)^3}\{&(\kappa-1)^2 (1-p_0)^{\kappa-1+2} - \left(2(\kappa-1)^2 + 2(\kappa-1) - 1\right)(1-p_0)^{\kappa-1+1} \\ &+ (\kappa-1+1)^2 (1-p_0)^{\kappa-1} - (1-p_0) - 1\} \end{aligned} \tag{68}$$

and reducing,

$$\begin{aligned} \sum_{i=0}^{\kappa-1} i^2 (1-p_0)^{i-1} = \frac{1}{(-p_0)^3}\{&(\kappa-1)^2 (1-p_0)^{\kappa+1} - \left(2(\kappa-1)^2 + 2(\kappa-1) - 1\right)(1-p_0)^{\kappa} \\ &+ (\kappa)^2 (1-p_0)^{\kappa-1} - (1-p_0) - 1\}. \end{aligned} \tag{69}$$

Combining terms and moving the negative into the bracketed term,

$$\sum_{i=0}^{\kappa-1} i^2 (1-p_0)^{i-1} = \frac{1}{(p_0)^3}\{1-(1-p_0)[(\kappa-1)^2(1-p_0)^{\kappa} - (2\kappa^2-2\kappa-1)(1-p_0)^{\kappa-1} + \kappa^2(1-p_0)^{\kappa-2}-1]\}. \quad (70)$$

Substituting (70) into (59),

$$E\left[\left(T_s^{nc}\right)^2\right] = (t_f)^2\, p_0 \frac{1}{(p_0)^3}\{1-(1-p_0)[(\kappa-1)^2(1-p_0)^{\kappa} - (2\kappa^2-2\kappa-1)(1-p_0)^{\kappa-1} + \kappa^2(1-p_0)^{\kappa-2}-1]\} + (\kappa t_f)^2(1-p_0)^{\kappa-1} \quad (71)$$

and pulling out the $\left(\frac{t_f}{p_0}\right)^2$ factor,

$$E\left[\left(T_s^{nc}\right)^2\right] = \left(\frac{t_f}{p_0}\right)^2 \{1-(1-p_0)[(\kappa-1)^2(1-p_0)^{\kappa} - (2\kappa^2-2\kappa-1)(1-p_0)^{\kappa-1} + \kappa^2(1-p_0)^{\kappa-2}-1] + \kappa^2 (p_0)^2 (1-p_0)^{\kappa-1}\}. \quad (72)$$

Combining terms, we finally arrive at the second moment of T_s^{nc} as

$$E\left[\left(T_s^{nc}\right)^2\right] = \left(\frac{t_f}{p_0}\right)^2 \{1-(1-p_0)[(\kappa-1)^2(1-p_0)^{\kappa} - (2\kappa^2-2\kappa-1)(1-p_0)^{\kappa-1} + \kappa^2\left(1-(p_0)^2\right)(1-p_0)^{\kappa-2}-1]\}. \quad (73)$$

The variance of the effective service time is defined as the square of the mean subtracted from the second moment or

$$VAR\left[\left(T_s^{nc}\right)\right] = E\left[\left(T_s^{nc}\right)^2\right] - \left(\bar{T}_s^{nc}\right)^2. \quad (74)$$

Substituting (56) and (73) into (74), we have

$$VAR\left[\left(T_s^{nc}\right)\right] = \left(\frac{t_f}{p_0}\right)^2 \{1-(1-p_0)[(\kappa-1)^2(1-p_0)^{\kappa} - (2\kappa^2-2\kappa-1)(1-p_0)^{\kappa-1} + \kappa^2\left(1-(p_0)^2\right)(1-p_0)^{\kappa-2}-1]\} - \left(\frac{t_f}{p_0}\right)^2 \left(1-(1-p_0)^{\kappa}\right)^2. \quad (75)$$

Factoring out the $\left(\frac{t_f}{p_0}\right)^2$ term and expanding,

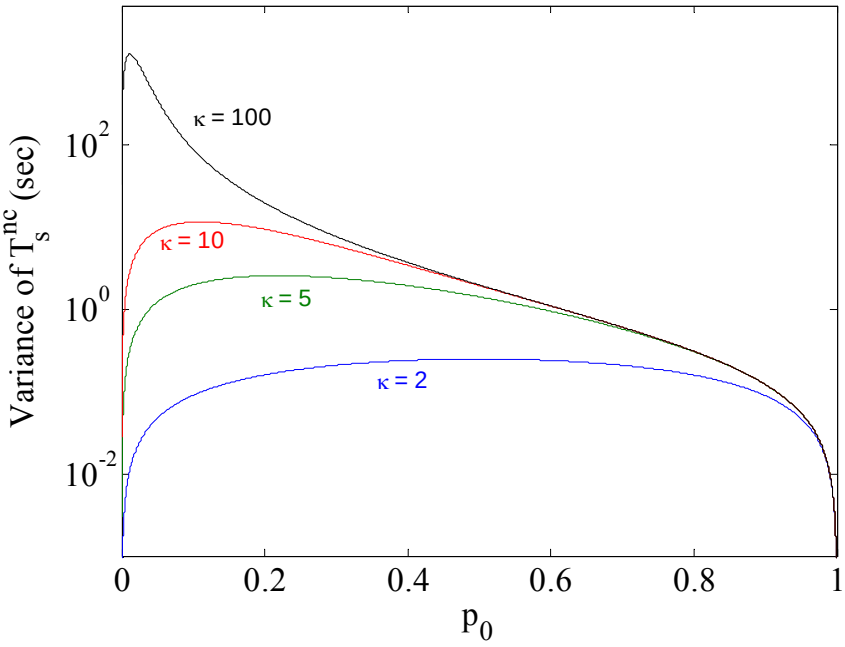

Figure 19. Variance of T_s^{nc} as a function of p_0 for various values of κ with $t_f = 1$ sec.

$$VAR\left[\left(T_s^{nc}\right)\right] = \left(\frac{t_f}{p_0}\right)^2 \{1-(1-p_0)[(\kappa-1)^2(1-p_0)^{\kappa} - (2\kappa^2-2\kappa-1)(1-p_0)^{\kappa-1} + \kappa^2\left(1-(p_0)^2\right)(1-p_0)^{\kappa-2} - 1] - \left(1-2(1-p_0)^{\kappa}+(1-p_0)^{2\kappa}\right)\}. \quad (76)$$

Combining terms, we finally arrive at

$$VAR\left[\left(T_s^{nc}\right)\right] = \left(\frac{t_f}{p_0}\right)^2 (1-p_0)[(1-p_0)^{2\kappa} + \left((\kappa-1)^2-1\right)(1-p_0)^{\kappa} - (2\kappa^2-2\kappa-1)(1-p_0)^{\kappa-1} + \kappa^2\left(1-(p_0)^2\right)(1-p_0)^{\kappa-2} - 1]. \quad (77)$$

Checking the limiting cases of $p_0 = 1$ (all non-contention slots) and $p_0 = 0$ (all contention slots), we find that the variance of T_s^{nc} is zero for both cases. This indicates that they are, as expected, deterministic. In the $p_0 = 0$ case, this result is arrived at through two applications of L'Hôpital's Rule. A plot of the variance of T_s^{nc} as a function of p_0 for various values of κ is provided in Figure 19.

We can now make use of the well-known mean waiting time result for an M/G/1 queue [9],

$$\bar{T}_w = \frac{\rho \bar{T}_s}{2(1-\rho)}\left(1+\left(\frac{VAR\left[\left(T_s\right)\right]}{\left(\bar{T}_s\right)^2}\right)\right) \tag{78}$$

where $\rho = \lambda \bar{T}_s < 1$. The latter term in (78), the variance over the mean squared for the service time, is often referred to as the square of the coefficient of variation and, in our case, from (56) and (77), is

$$\begin{aligned}\frac{VAR\left[\left(T_s^{nc}\right)\right]}{\left(\bar{T}_s^{nc}\right)^2} = \left(\frac{1-p_0}{\left(1-\left(1-p_0\right)^{\kappa}\right)^2}\right)[&\left(1-p_0\right)^{2\kappa} + \left(\left(\kappa-1\right)^2-1\right)\left(1-p_0\right)^{\kappa} \\ &-\left(2\kappa^2-2\kappa-1\right)\left(1-p_0\right)^{\kappa-1} \\ &+\kappa^2\left(1-\left(p_0\right)^2\right)\left(1-p_0\right)^{\kappa-2}-1].\end{aligned} \tag{79}$$

A value of zero for the coefficient of variation indicates that the service time is deterministic while a value of one indicates that it is exponential [9]. Since the variance is zero and the mean of the square is non-zero in the limiting cases of $p_0 = 1$ and $p_0 = 0$, the coefficient of variation in (79) is zero in both cases, as expected. A plot of the coefficient of variation of T_s^{nc} as a function of p_0 for various values of κ is provided in Figure 20. Interestingly, the coefficient of variation is less than zero and approaches one as p_0 becomes small and κ becomes large. Thus, the distribution of the service time approaches exponential as the probability of a non-contention slot decreases and ratio of T_{data} for the non-contention slot to that for a contention slot increases.

Finally, from (55), we can substitute

$$\rho_{nc} = \lambda_{nc}\bar{T}_s^{nc} = \lambda_{nc}\left(\frac{1-\left(1-p_0\right)^{\kappa}}{p_0}\right) < 1 \tag{80}$$

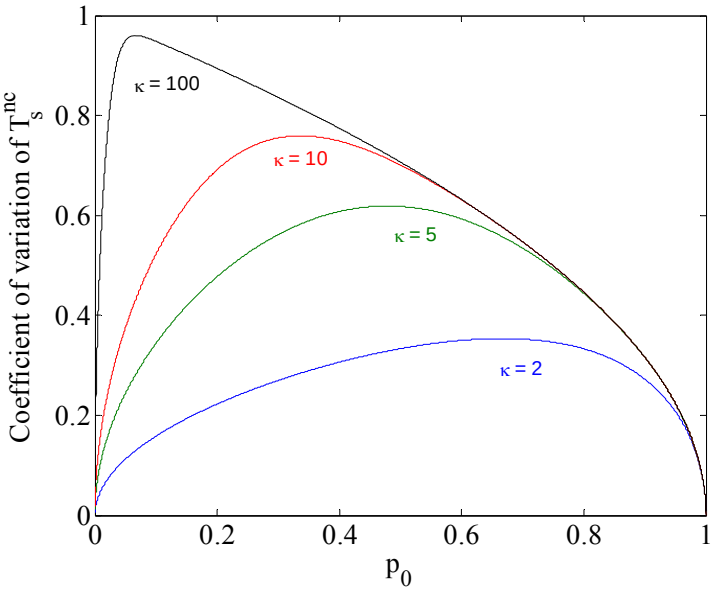

Figure 20. Coefficient of variation of T_s^{nc} as a function of p_0 for various values of κ.

into (78) to arrive at

$$\bar{T}_w^{nc} = \frac{\lambda_{nc}\left(\frac{1-(1-p_0)^{\kappa}}{p_0}\right)^2}{2\left(1-\lambda_{nc}\left(\frac{1-(1-p_0)^{\kappa}}{p_0}\right)\right)}\left(1+\left(\frac{VAR\left[(T_s)\right]}{(\bar{T}_s)^2}\right)\right). \tag{81}$$

Again, looking at the limiting cases, we find that

$$\lim_{p_0\to 1}\bar{T}_w^{nc} = \frac{\lambda_{nc}(t_f)^2}{2(1-\lambda_{nc}t_f)} \qquad \text{and}$$
$$\lim_{p_0\to 0}\bar{T}_w^{nc} = \frac{\lambda_{nc}(\kappa t_f)^2}{2(1-\lambda_{nc}\kappa t_f)} \tag{82}$$

which agree with the deterministic case solved by Lam in [7]. A plot of $\bar{T}_w^{nc}$ as a function of p_0 for various values of κ is provided in Figure 21, while a plot of $\bar{T}_w^{nc}$ as a function of ρ_{nc} for various values of p_0 is provided in Figure 22.

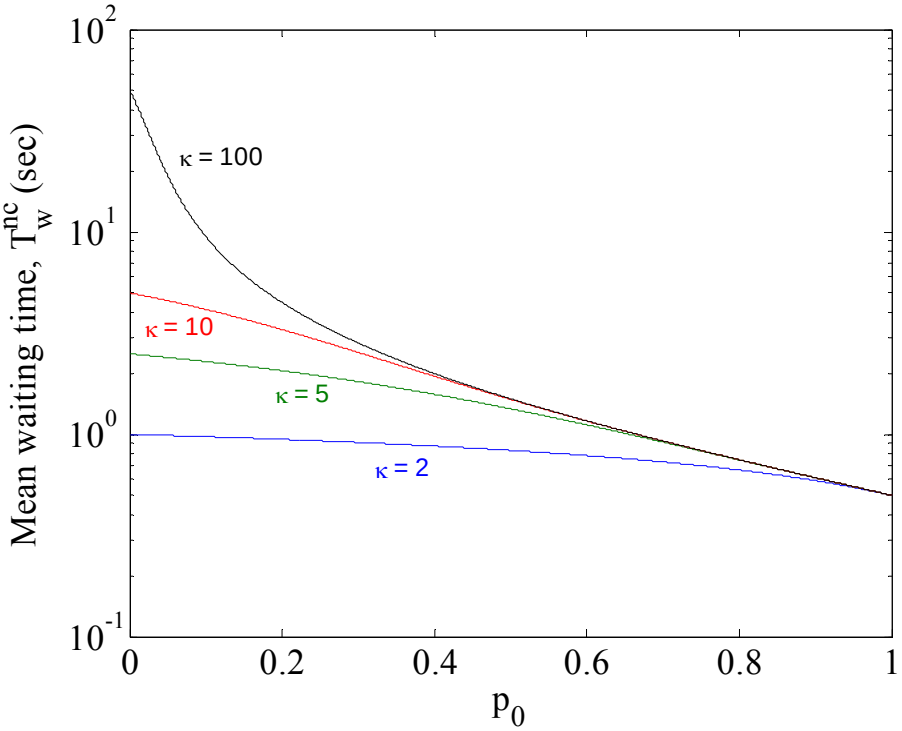

Figure 21. $\bar{T}_w^{nc}$ as a function of p_0 for various values of κ with $t_f = 1$ sec.

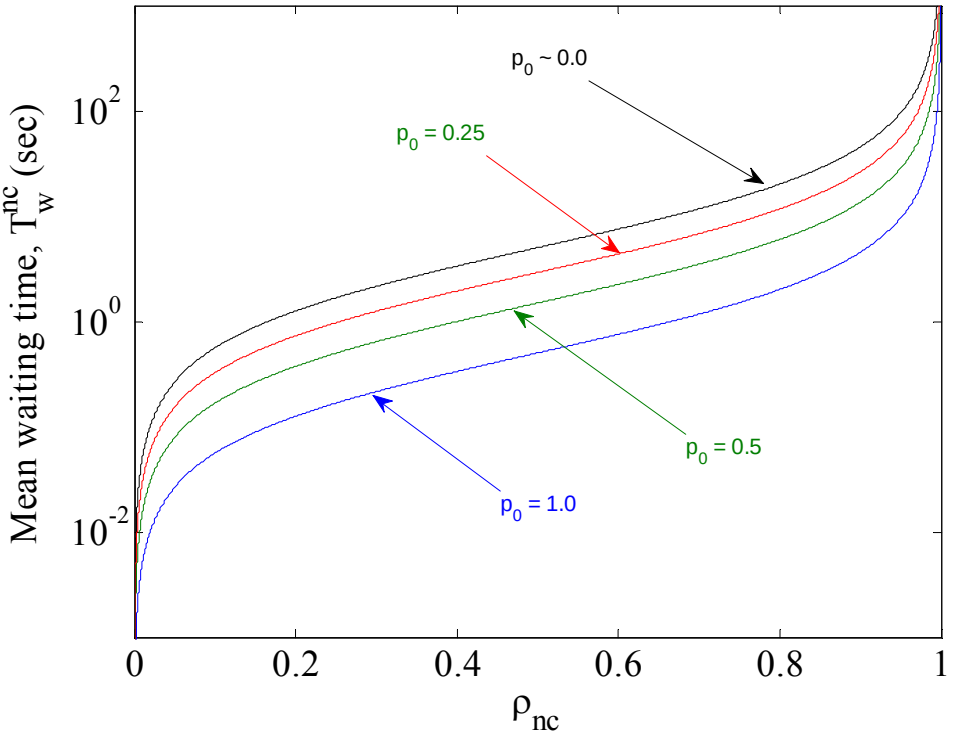

Figure 22. $\bar{T}_w^{nc}$ as a function of ρ_{nc} for various values of p_0 with $t_f = 1$ sec.

Turning our attention to $\overline{T}_{xmt}^{nc}$, this is simply the mean time required to transmit a packet once its waiting time is complete. We begin by calculating $\overline{T}_{xmt}^{nc}$ for a packet that is transmitted in a single non-contention slot, denoted $T_{xmt_1}^{nc}$. Again assuming that exactly one non-contention packet is transmitted during a non-contention slot, the transmission time for a packet transmitted in a non-contention slot is, from (22),

$$T_{xmt_1}^{nc} = t_{IFS} + t_{nc} \tag{83}$$

where t_{IFS} is included to account for the delay between the slot boundary and the actual start of the transmission. For a packet that is transmitted in a contention slot, the actual transmission will span across frames, as discussed above. Examining the case where a packet is transmitted in a contention slot followed by a non-contention slot, denoted $T_{xmt_2}^{nc}$,we have, again from (22),

$$T_{xmt_2}^{nc} = t_f + \left(t_{IFS} + t_{nc}\right) - \left(t_{nc} + t_{IFS} - t_b - kt_{ms}\right) \tag{84}$$

where, as in (83), the first term t_f accounts for the single frame time to get to the second (non-contention) slot, the second term $\left(t_{IFS} + t_{nc}\right)$ accounts for the packet transmission in this final non-contention slot, and the third term $\left(t_{nc} + t_{IFS} - t_b - kt_{ms}\right)$ reduces the transmission time required in this final non-contention slot by the amount of the packet that was transmitted in the prior contention slot. Extending this argument to the general case in which we have $\alpha - 1$ consecutive contention slots followed by a non-contention slot, where $\alpha \le \kappa$ in (38),

$$T_{xmt_\alpha}^{nc} = (\alpha - 1)t_f + \left(t_{IFS} + t_{nc}\right) - (\alpha - 1)\left(t_{nc} + t_{IFS} - t_b - kt_{ms}\right). \tag{85}$$

Following the development of (39), the probability $T_{xmt_\alpha}^{nc}$ is a function of both α and p_0 and is given by

$$\Pr\left[T_{xmt}^{nc} = T_{xmt_\alpha}^{nc}\right] = p_0\left(1 - p_0\right)^{\alpha - 1} \qquad \text{for } 1 \le \alpha \le \kappa. \tag{86}$$

Here, as opposed to (39), we have included κ in the range of α because we must explicitly account for the case of $\kappa - 1$ consecutive contention slots followed by a non-contention slot as well as the case of κ consecutive contention slots. For this latter case, we have

$$T_{xmt_{\kappa c}}^{nc} = (\kappa - 1)t_f + (t_b + kt_{ms}) + \left[t_{nc} - (\kappa - 1)t_{nc2}\right] \tag{87}$$

where the second term $(t_b + kt_{ms})$ now accounts for the fact that the final slot is a contention slot and we have defined $t_{nc2} = t_{nc} + t_{IFS} - t_b - kt_{ms}$. The probability of this case is

$$\Pr\left[T_{xmt}^{nc} = T_{xmt_{\kappa c}}^{nc}\right] = (1 - p_0)^{\kappa}. \tag{88}$$

We can calculate the mean transmission time $\bar{T}_{xmt}^{nc}$ by combining (85) through (88) which, after a little algebraic manipulation, is

$$\begin{aligned} \bar{T}_{xmt}^{nc} = &\sum_{i=1}^{\kappa}\left[(i-1)(t_f - t_{nc2}) + t_{IFS} + t_{nc}\right]p_0(1-p_0)^{i-1} \\ &+\left[(\kappa-1)(t_f - t_{nc2}) + t_b + kt_{ms} + t_{nc}\right](1-p_0)^{\kappa}. \end{aligned} \tag{89}$$

Rearranging terms,

$$\begin{aligned} \bar{T}_{xmt}^{nc} = &\sum_{i=1}^{\kappa}\left[i(t_f - t_{nc2}) - (t_f - (t_{IFS} + t_{nc} + t_{nc2}))\right]p_0(1-p_0)^{i-1} \\ &+\left[(\kappa-1)(t_f - t_{nc2}) + t_b + kt_{ms} + t_{nc}\right](1-p_0)^{\kappa} \end{aligned} \tag{90}$$

and distributing,

$$\begin{aligned} \bar{T}_{xmt}^{nc} = p_0&\sum_{i=1}^{\kappa}\left[i(t_f - t_{nc2})(1-p_0)^{i-1} - (t_f - (t_{IFS} + t_{nc} + t_{nc2}))(1-p_0)^{i-1}\right] \\ &+\left[(\kappa-1)(t_f - t_{nc2}) + t_b + kt_{ms} + t_{nc}\right](1-p_0)^{\kappa}. \end{aligned} \tag{91}$$

Pulling the appropriate terms out of the summation and distributing it across,

$$\begin{aligned} \bar{T}_{xmt}^{nc} = &(t_f - t_{nc2})\,p_0\sum_{i=1}^{\kappa} i(1-p_0)^{i-1} \\ &-(t_f - (t_{IFS} + t_{nc} + t_{nc2}))\,p_0\sum_{i=1}^{\kappa}(1-p_0)^{i-1} \\ &+\left[(\kappa-1)(t_f - t_{nc2}) + t_b + kt_{ms} + t_{nc}\right](1-p_0)^{\kappa}. \end{aligned} \tag{92}$$

Adjusting the indices on the summations,

$$\begin{aligned} \bar{T}_{xmt}^{nc} = &(t_f - t_{nc2})\,p_0\sum_{i=0}^{\kappa} i(1-p_0)^{i-1} \\ &-(t_f - (t_{IFS} + t_{nc} + t_{nc2}))\,p_0\sum_{j=0}^{\kappa-1}(1-p_0)^{j} \\ &+\left[(\kappa-1)(t_f - t_{nc2}) + t_b + kt_{ms} + t_{nc}\right](1-p_0)^{\kappa} \end{aligned} \tag{93}$$

and using (42), (67) and the appropriate substitutions, we have

$$\begin{aligned}\bar{T}_{xmt}^{nc} &= \left(t_f - t_{nc2}\right) p_0 \frac{\left(\kappa+1\right)\left(1-p_0\right)^{\kappa}\left(\left(1-p_0\right)-1\right)-\left(\left(1-p_0\right)^{\kappa+1}-1\right)}{\left(\left(1-p_0\right)-1\right)^2} \\ &\quad -\left(t_f - \left(t_{IFS}+t_{nc}+t_{nc2}\right)\right) p_0 \frac{\left(1-p_0\right)^{\kappa-1+1}-1}{1-p_0-1} \\ &\quad +\left[\left(\kappa-1\right)\left(t_f - t_{nc2}\right)+t_b+kt_{ms}+t_{nc}\right]\left(1-p_0\right)^{\kappa}.\end{aligned} \tag{94}$$

Simplifying and rearranging terms,

$$\begin{aligned}\bar{T}_{xmt}^{nc} &= \left(t_f - t_{nc2}\right)\frac{\left(\kappa+1\right)\left(1-p_0\right)^{\kappa+1}-\left(\kappa+1\right)\left(1-p_0\right)^{\kappa}-\left(1-p_0\right)^{\kappa+1}+1}{p_0} \\ &\quad -\left(t_f - \left(t_{IFS}+t_{nc}+t_{nc2}\right)\right) p_0 \frac{\left(1-p_0\right)^{\kappa}-1}{\left(-p_0\right)} \\ &\quad +\left[\left(\kappa-1\right)\left(t_f - t_{nc2}\right)+t_b+kt_{ms}+t_{nc}\right]\left(1-p_0\right)^{\kappa}\end{aligned} \tag{95}$$

and further algebraic manipulation leads to

$$\begin{aligned}\bar{T}_{xmt}^{nc} &= \left[t_f - t_{nc2}\right]\left(\frac{\kappa\left(1-p_0\right)^{\kappa+1}-\left(\kappa+1\right)\left(1-p_0\right)^{\kappa}+1}{p_0}\right) \\ &\quad -\left[t_f - \left(t_{IFS}+t_{nc}+t_{nc2}\right)\right]\left(1-\left(1-p_0\right)^{\kappa}\right) \\ &\quad +\left[\left(\kappa-1\right)\left(t_f - t_{nc2}\right)+t_b+kt_{ms}+t_{nc}\right]\left(1-p_0\right)^{\kappa}.\end{aligned} \tag{96}$$

Expanding,

$$\begin{aligned}\bar{T}_{xmt}^{nc} &= \left[t_f - t_{nc2}\right]\left(\frac{\kappa\left(1-p_0\right)^{\kappa+1}-\left(\kappa+1\right)\left(1-p_0\right)^{\kappa}+1}{p_0}\right) \\ &\quad +\left[\kappa\left(t_f - t_{nc2}\right)-t_f+t_{nc2}+t_b+kt_{ms}+t_{nc}+t_f-t_{IFS}-t_{nc}-t_{nc2}\right]\left(1-p_0\right)^{\kappa} \\ &\quad -t_f+t_{IFS}+t_{nc}+t_{nc2}\end{aligned} \tag{97}$$

and, finally, simplifying to arrive at

$$\begin{aligned}\bar{T}_{xmt}^{nc} &= \left[t_f - t_{nc2}\right]\left(\frac{\kappa\left(1-p_0\right)^{\kappa+1}-\left(\kappa+1\right)\left(1-p_0\right)^{\kappa}+1}{p_0}\right) \\ &\quad +\left[\kappa\left(t_f - t_{nc2}\right)-t_{IFS}+t_b+kt_{ms}\right]\left(1-p_0\right)^{\kappa} \\ &\quad -t_f+t_{IFS}+t_{nc}+t_{nc2}.\end{aligned} \tag{98}$$

Checking the limiting cases of $p_0 = 1$ (all non-contention slots) and $p_0 = 0$ (all contention slots), we obtain the expected results from (83) and (87) of

$$\begin{aligned} &\lim_{p_0 \to 1} \bar{T}_{xmt}^{nc} = t_{IFS} + t_{nc} \qquad \text{and} \\ &\lim_{p_0 \to 0} \bar{T}_{xmt}^{nc} = (\kappa - 1) t_f + t_b + \kappa t_{ms} + \left[t_{nc} - (\kappa - 1) t_{nc2} \right]. \end{aligned} \tag{99}$$

The latter result is arrived at through a single application of L'Hôpital's Rule. A plot of the mean transmission time as a function of p_0 for various values of κ is provided in Figure 23.

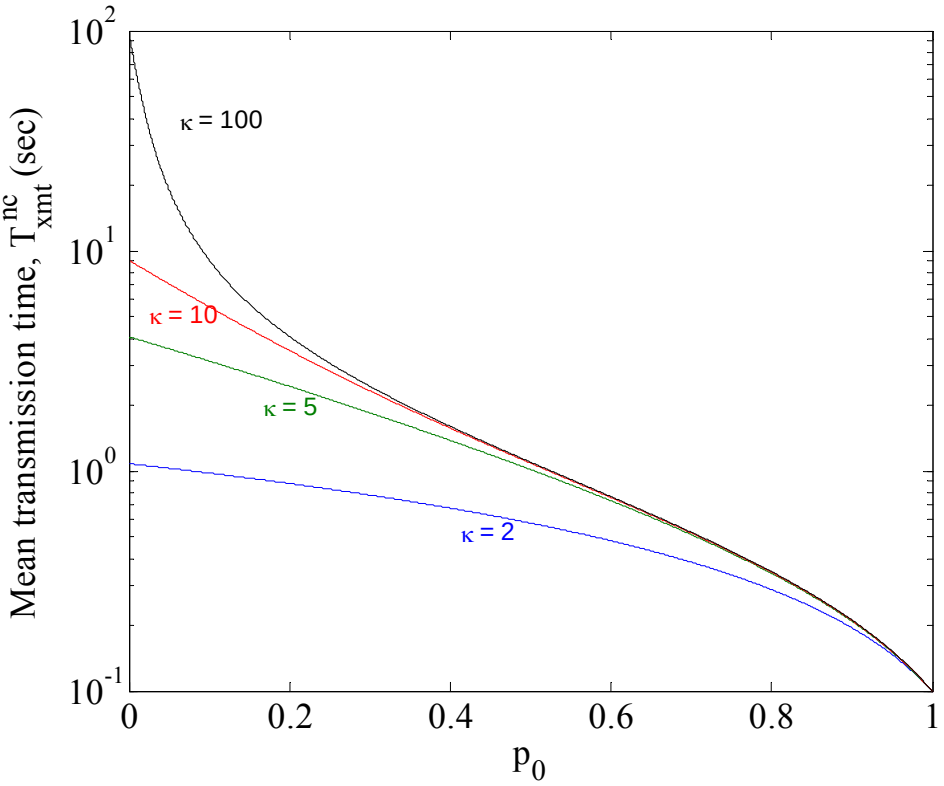

Figure 23. The mean transmission time as a function of p_0 for various values of κ with $t_f = 1$ sec.

We can finally arrive at an expression for the total mean packet delay for the contention mode by substituting (36), (81), and (98) into (35),

$$\bar{D}^{nc} = \frac{t_s}{2} + \frac{\lambda_{nc}\left(\frac{1-(1-p_0)^{\kappa}}{p_0}\right)^2}{2\left(1-\lambda_{nc}\left(\frac{1-(1-p_0)^{\kappa}}{p_0}\right)\right)}\left(1+\left(\frac{VAR\left[(T_s)\right]}{(\bar{T}_s)^2}\right)\right)$$
$$+\left[t_f - t_{nc2}\right]\left(\frac{\kappa(1-p_0)^{\kappa+1} - (\kappa+1)(1-p_0)^{\kappa} + 1}{p_0}\right) \qquad (100)$$
$$+\left[\kappa\left(t_f - t_{nc2}\right) - t_{IFS} + t_b + kt_{ms}\right](1-p_0)^{\kappa}$$
$$-t_f + t_{IFS} + t_{nc} + t_{nc2} + t_{prop}$$

where

$$\frac{VAR\left[\left(T_s^{nc}\right)\right]}{\left(\bar{T}_s^{nc}\right)^2} = \left(\frac{1-p_0}{\left(1-(1-p_0)^{\kappa}\right)^2}\right)[(1-p_0)^{2\kappa} + \left((\kappa-1)^2 - 1\right)(1-p_0)^{\kappa}$$
$$-\left(2\kappa^2 - 2\kappa - 1\right)(1-p_0)^{\kappa-1} \qquad . \qquad (101)$$
$$+\kappa^2\left(1-(p_0)^2\right)(1-p_0)^{\kappa-2} - 1].$$

A plot of the mean total packet delay as a function of p_0 for various values of κ is provided in Figure 24, while it is plotted as a function of ρ_{nc} for various values of p_0 is provided in Figure 25. Finally, it is plotted in Figure 26 as a function of the aggregate non-contention load, Λ_{nc}, for various values of p_0.

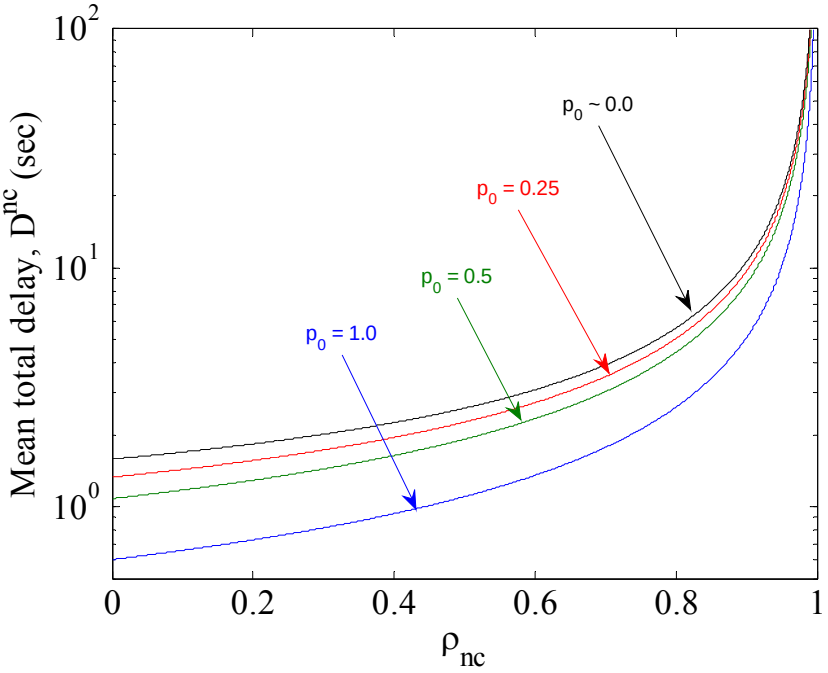

Figure 24. Non-contention mode mean total packet delay as a function of ρ_{nc} for various values of p_0 with $t_f = 1$ sec.

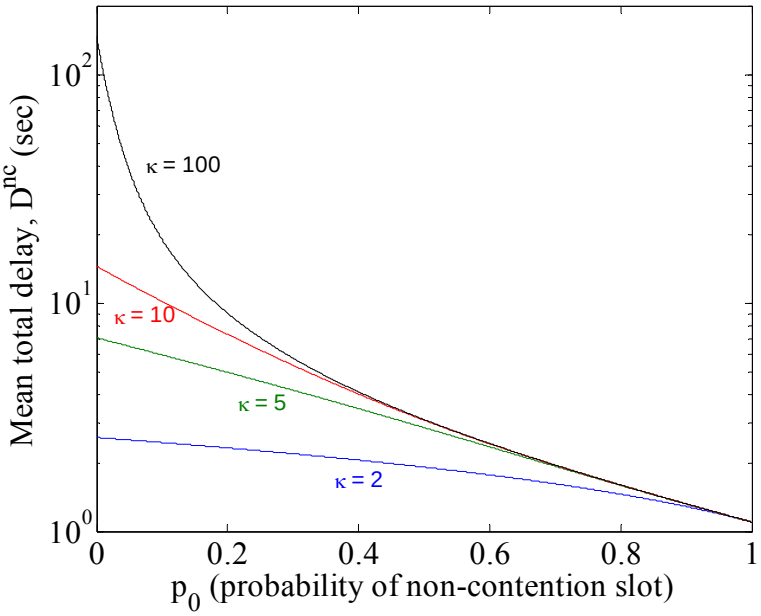

Figure 25. Non-contention mode mean total packet delay as a function of p_0 for various values of κ with $t_f = 1$ sec.

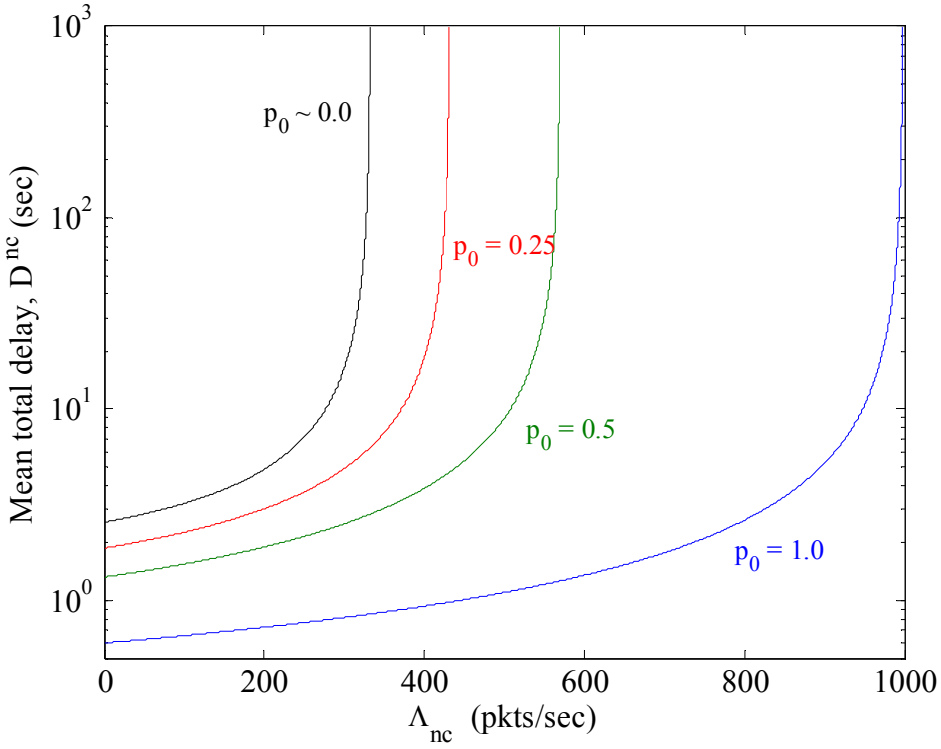

Figure 26. Non-contention mode mean total packet delay as a function of Λ_{nc} (aggregate packet arrival rate) for various values of p_0 with $t_f = 1$ sec.

3. Slotted Aloha model with periodic server vacations

We begin our analysis of the contention mode by developing a model for a Slotted Aloha system with periodic server vacations. By this we mean that the service will be governed by a fixed cycle composed of alternating active and inactive periods. During the inactive period, the server will "shut down" and not be available to serve the queued packets. We also make the assumption that once a server has entered an active period, all subsequent packet arrivals will be deferred to the next active period (i.e., a packet must arrive prior to an active period to be eligible for service in that period). We define K as the number of slots in an active period. Following the work of [20] and [19], we make use of the model in Figure 27. Here, a node attempts transmission in a given slot with probability p and, if the transmission is unsuccessful, the packet is requeued.

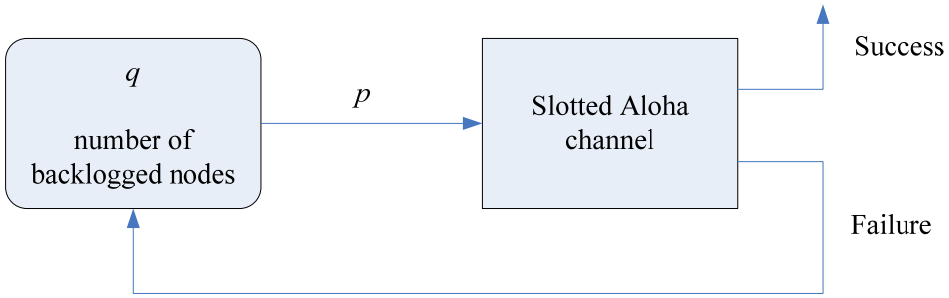

Figure 27. Model of a slotted ALOHA channel with q backlogged nodes [after [19]].

To develop the associated discrete Markov chain, we define a state by the number of nodes with a packet queued for transmission and derive the associated state transition probability matrix, P. We define $p_{i,j}$ as the probability that the system will transition from state i to state j in a given slot. We begin by recognizing that the probability of a transition from i to j where $j > i$ is zero during the active period because we have assumed that all additional arrivals are deferred to the next active period. Furthermore, the probability of a transition where $j < i-1$ is also zero because there can only be at most one successful transmission per slot. The case of $j = i+1$ represents a single successful transmission. This will occur when any one of the i nodes with a packet queued attempts to transmit and all of the other nodes do not. Since a node will attempt a transmission with probability p, this is simply

$$p_{i,i-1} = \binom{i}{1} p(1-p)^{i-1} = ip(1-p)^{i-1}. \tag{102}$$

This leaves the probability that a node will remain in the current state which is

$$p_{i,i} = 1 - p_{i,i-1} = 1 - ip(1-p)^{i-1}. \tag{103}$$

Combining these, we have

$$p_{i,j} = \begin{cases} 0 & j < i-1 \\ ip(1-p)^{i-1} & j = i-1 \\ 1-ip(1-p)^{i-1} & j = i \\ 0 & j > i \end{cases}. \tag{104}$$

Defining $\sigma = p(1-p)^{i-1}$, the corresponding $(M+1)\times(M+1)$ probability transition matrix is

$$\mathrm{P} = \begin{bmatrix} 1-\sigma & 0 & 0 \\ \sigma & \ddots & 0 \\ 0 & \sigma & 1-\sigma \end{bmatrix} \tag{105}$$

where M is the number of nodes with a packet queued for transmission at the start of the active period.

The state probability vector $\underline{p}(k)$ is defined as

$$\underline{p}(k) = \begin{bmatrix} p_0(k) \\ p_1(k) \\ \vdots \\ p_M(k) \end{bmatrix}^T \tag{106}$$

where $p_i(k)$ is the probability of state i at the end of slot k and X^T is the transpose of X. Thus, for the resulting Markov chain in Figure 28,

$$\begin{aligned} \underline{p}(1) &= \underline{p}(0)\,\mathrm{P}, \\ \underline{p}(2) &= \underline{p}(1)\,\mathrm{P} = \left(\underline{p}(0)\,\mathrm{P}\right)\mathrm{P} = \underline{p}(0)\,\mathrm{P}^2, \end{aligned} \tag{107}$$

and

$$\underline{p}(k) = \underline{p}(0)\,\mathrm{P}^k = \underline{p}(0)\begin{bmatrix} 1-\sigma & 0 & 0 \\ \sigma & \ddots & 0 \\ 0 & \sigma & 1-\sigma \end{bmatrix}^k \tag{108}$$

where $\underline{p}(0)$ is the initial state probability vector at the start of the active period. Note that the mean number of nodes with packets queued in a given slot k, denoted $Q(k)$, is simply the mean of the appropriate state probability vector as in

$$Q(k) = \underline{p}(k)\begin{bmatrix} 0 \\ 1 \\ \vdots \\ M \end{bmatrix} = \underline{p}(0)\begin{bmatrix} 1-\sigma & 0 & 0 \\ \sigma & \ddots & 0 \\ 0 & \sigma & 1-\sigma \end{bmatrix}^k \begin{bmatrix} 0 \\ 1 \\ \vdots \\ M \end{bmatrix}. \tag{109}$$

For an active period of K slots, the state probability vector at the end of the active period is given by

$$\underline{p}(K) = \underline{p}(0)\,\mathrm{P}^K = \underline{p}(0)\begin{bmatrix} 1-\sigma & 0 & 0 \\ \sigma & \ddots & 0 \\ 0 & \sigma & 1-\sigma \end{bmatrix}^K . \tag{110}$$

and the mean number of nodes with packets queued at the end of an active period is $Q(K)$.

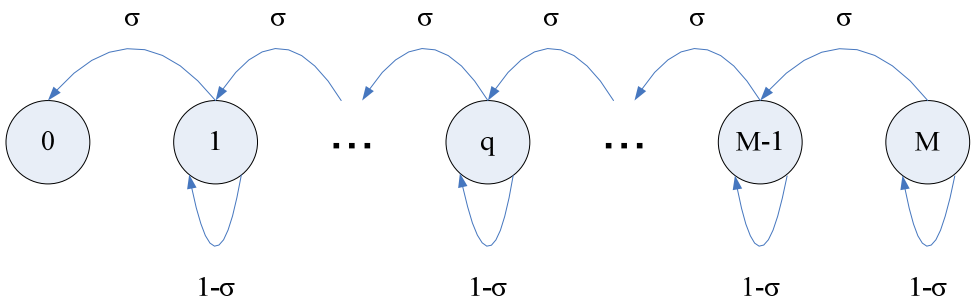

Figure 28. Markov chain for Slotted Aloha with server vacations.

For a cycle time (defined as one active period followed by one inactive period) of duration T_{cycle} and an arrival rate of λ, the initial mean number of nodes with packets queued at the start of the next active period, denoted $Q'(0)$, is

$$Q'(0) = Q(K) + \lambda T_{cycle} . \tag{111}$$

We then define steady state as the condition where $\underline{p}'(k) = \underline{p}(k)$ which implies that

$$Q'(0) = Q(0),\ Q'(K) = Q(K) \tag{112}$$

and, from (111),

$$Q(0) - Q(K) = \lambda T_{cycle} . \tag{113}$$

We now use the results from this model to derive the throughput and delay for slotted ALOHA with periodic server vacations.

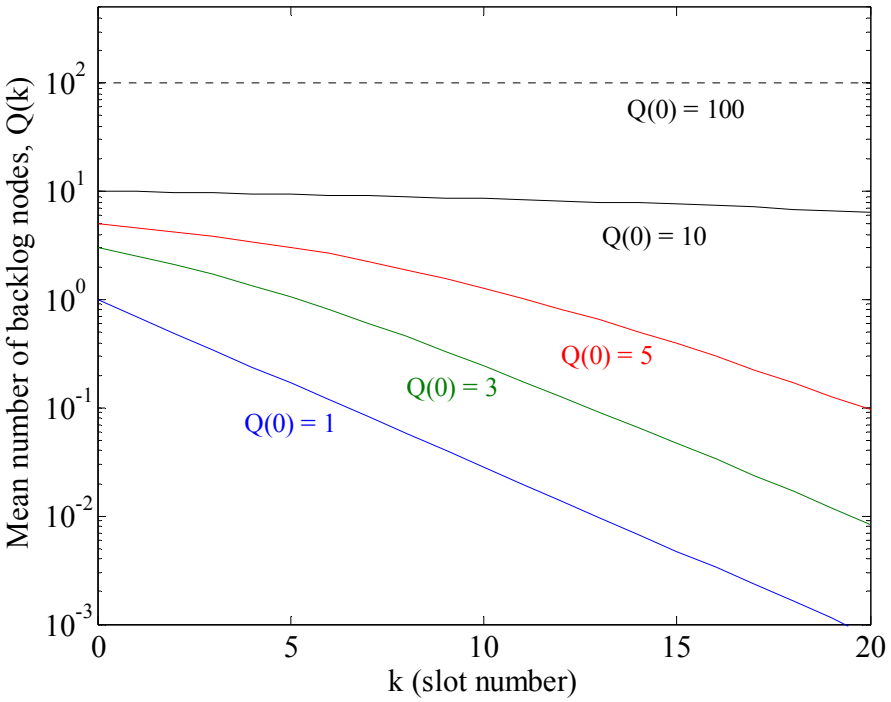

Figure 29. Mean number of backlogged nodes (nodes with a packet queued for transmission) as a function of slot number for various initial state conditions. For this plot, the probability of transmission in a slot, *p*, is 0.3.

4. Throughput for Slotted Aloha with periodic server vacations

The throughput for slotted ALOHA with periodic server vacations is then simply the difference between the mean number of nodes with packets queued at the beginning of an active period and the mean number at the end of the active period divided by the cycle time, or

$$\text{Throughput} = \frac{Q(0) - Q(K)}{T_{cycle}}. \tag{114}$$

From (113), this implies, as expected, that the throughput at steady state equals the arrival rate. To be consistent with the literature, we can normalize (114) by multiplying it by the packet transmission time T_{xmt}^{c} to arrive at

$$S^{c} = \frac{Q(0) - Q(K)}{T_{cycle}} T_{xmt}^{c}. \tag{115}$$

We plot the throughput as a function of the offered load $Q(0)$ in Figure 30 for various values of κ.

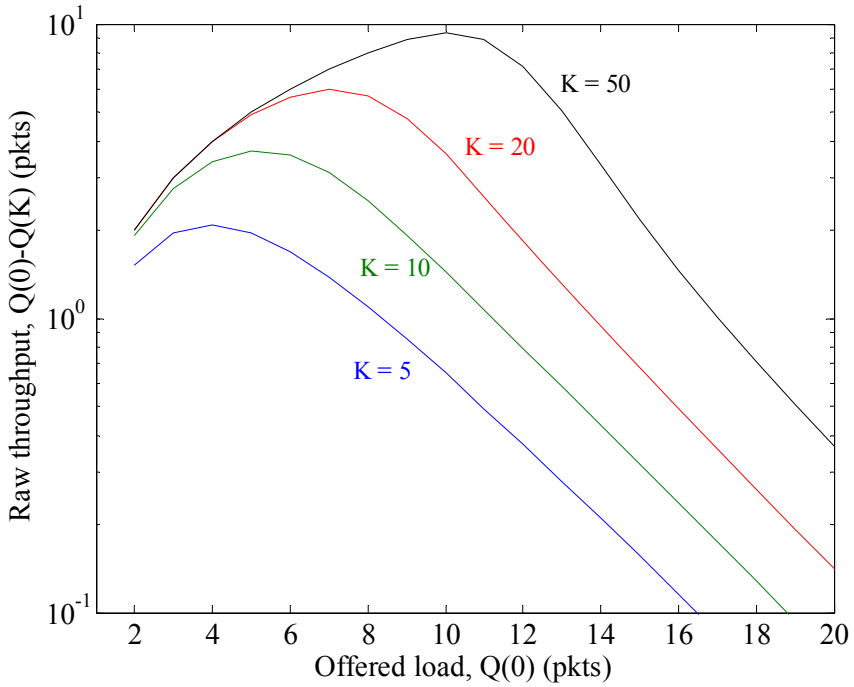

Figure 30. Raw throughput per active period as a function of offered load for various number of slots per active period (K). For this plot, the probability of transmission in a slot, p, is 0.3.

5. Delay for Slotted Aloha with periodic server vacations

As in (35), we can calculate the mean total packet delay for slotted ALOHA with periodic server vacations as the sum of (1) the mean time to synchronize to an active period, (2) the mean waiting time, (3) the mean transmission time and (4) the mean propagation time or

$$\overline{D} = \overline{T}_{sync} + \overline{T}_{w} + \overline{T}_{xmt} + t_{prop} . \tag{116}$$

The first term can be calculated as in (36) to be

$$\overline{T}_{sync} = \frac{T_{cycle}}{2} . \tag{117}$$

and, because we are assuming that a packet can be transmitted in a single slot,

$$\overline{T}_{xmt} = \frac{\overline{L}}{R} \tag{118}$$

where $\overline{L}$ is the mean packet length (in bits) and R is the channel data rate (bps).

Turning our attention once again to the waiting time, we view the entire system as a single M/G/1 queue and we develop the service time distribution using the model

developed above. A packet transmitted in the first slot of the active period will experience a service time of T_{xmt} while a packet transmitted in the second slot will wait through the first slot and then transmit for a service time of $T_{slot} + T_{xmt}$. This can be generalized for slot *k* in the active period as

$$T_s(k) = (k-1)T_{slot} + T_{ovhd} + T_{xmt} \tag{119}$$

where we have included the overhead T_{ovhd} in the transmission slot. A packet can also wait across active periods as well. This would occur if the probability of at least one packet queued for transmission at the end of an active period was non-zero. Following the same logic, then, a packet that is transmitted in the m^{th} active period would have to wait an additional $m-1$ cycle times or

$$T_s(m,k) = (m-1)T_{cycle} + (k-1)T_{slot} + T_{ovhd} + T_{xmt}. \tag{120}$$

Thus, the service time is a discrete random variable that can take on the values indicated in (120). To develop the distribution, we must now calculate the probabilities of the discrete values.

The probability that a packet will be successfully transmitted in the first slot of an active period is the probability that one node will transmit and that the remaining $Q(0)-1$ nodes will not. Since a node transmits in a slot with probability *p*, this probability is

$$\Pr[T_s = T_s(0,1)] = p(1-p)^{Q(0)-1}. \tag{121}$$

The probability that a node will successfully be transmitted in the second slot of an active period is the probability that it wasn't successfully transmitted in the multiplied by the probability that it is transmitted in the second slot and none of the other $Q(1)-1$ nodes transmit or

$$\Pr[T_s = T_s(0,2)] = \left(1 - p(1-p)^{Q(0)-1}\right) p(1-p)^{Q(1)-1}. \tag{122}$$

Looking at the next slot, we must include the probability that it was not successfully transmitted in either of the first two slots as in

$$\Pr[T_s = T_s(0,3)] = \left[1 - p(1-p)^{Q(0)-1} - \left(1 - p(1-p)^{Q(0)-1}\right) p(1-p)^{Q(1)-1}\right] p(1-p)^{Q(2)-1} \tag{123}$$

or, rewriting it as a recursion,

$$\Pr[T_s = T_s(0,3)] = 1 - (\Pr[T_s = T_s(0,1)] + \Pr[T_s = T_s(0,2)])\, p\left(1-p\right)^{Q(3)-1}. \qquad (124)$$

Extending this by induction to the general case in the first active period, we have

$$\Pr[T_s = T_s(0,k)] = \left(1 - \sum_{i=1}^{k-1} \Pr[T_s = T_s(0,i)]\right) p\left(1-p\right)^{Q(k-1)-1}. \qquad (125)$$

Assuming steady state (i.e. $Q'(k) = Q(k)$), we can also extend this across cycles by adding a second summation as in

$$\Pr[T_s = T_s(m,k)] = \left(1 - \sum_{j=0}^{m-1} \sum_{i=1}^{k-1} \Pr[T_s = T_s(j,i)]\right) p\left(1-p\right)^{Q(k-1)-1}. \qquad (126)$$

This is a recursive equation and can be solved numerically to some desired level of accuracy. The distribution of T_s is then defined by (120) and (126) and we can also numerically calculate its mean and variance to some desired degree of accuracy. The probability distribution and cumulative distribution function for the service time of slotted ALOHA with periodic server vacations are plotted in Figures 31 through 34.

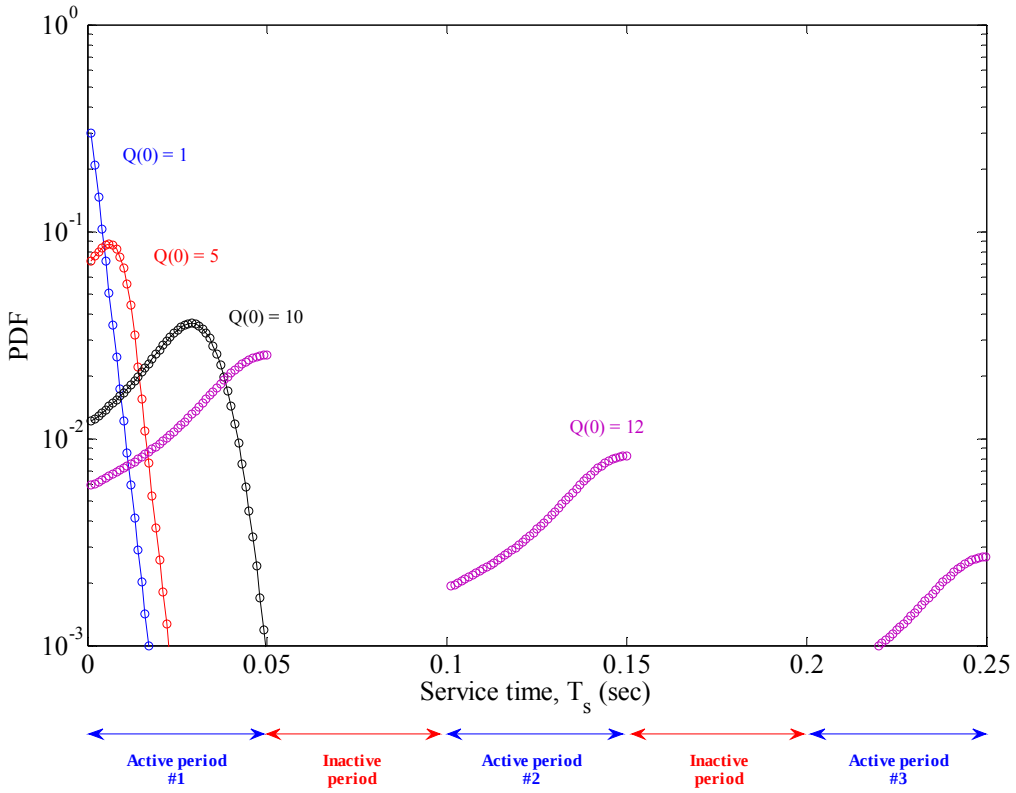

Figure 31. Service time probability distribution in log-linear scale. For this plot, the probability of transmission in a slot, p, is 0.3.

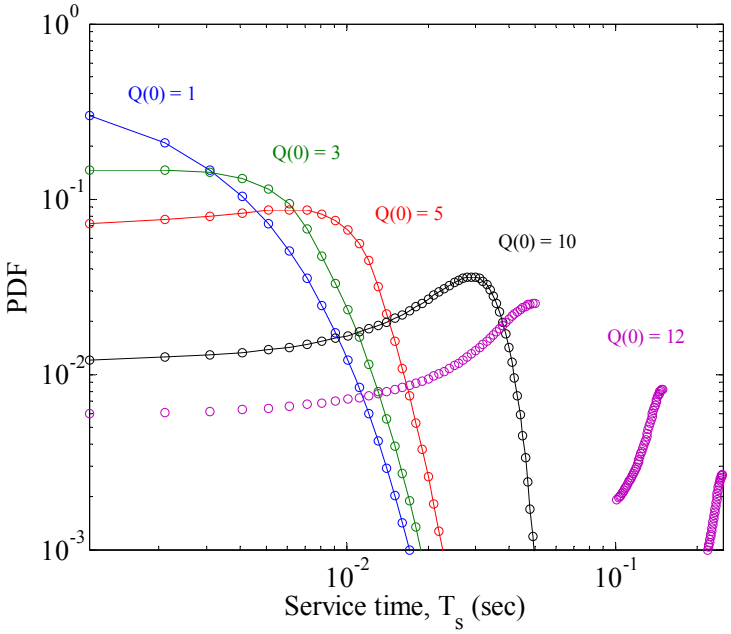

Figure 32. Service time probability distribution in log-log scale. For this plot, the probability of transmission in a slot, *p*, is 0.3.

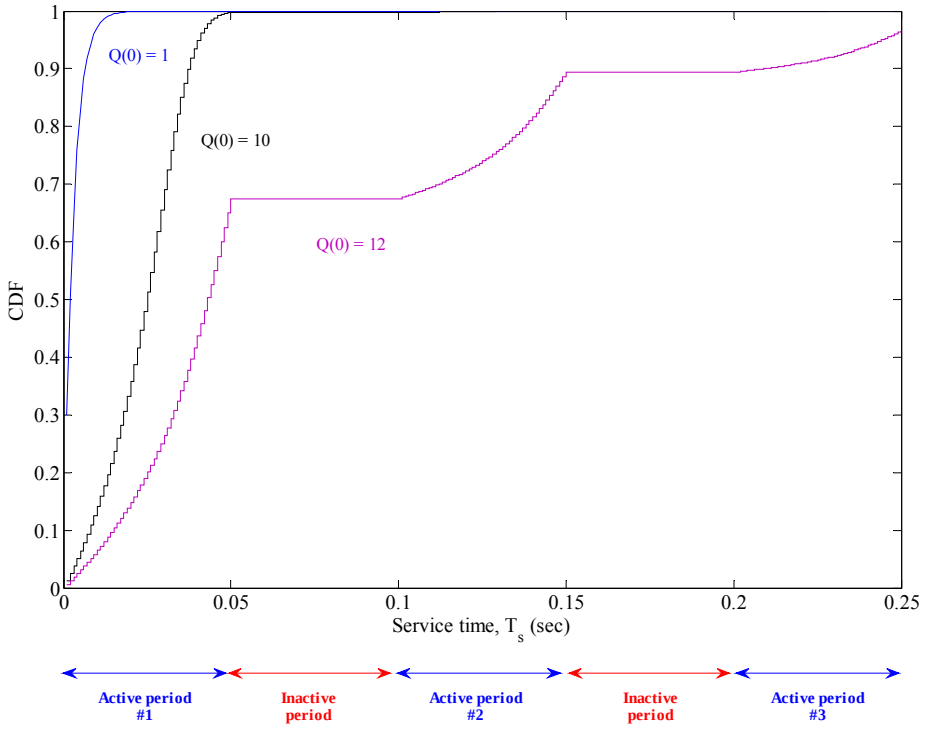

Figure 33. Service time cumulative distribution in linear scale. For this plot, the probability of transmission in a slot, *p*, is 0.3.

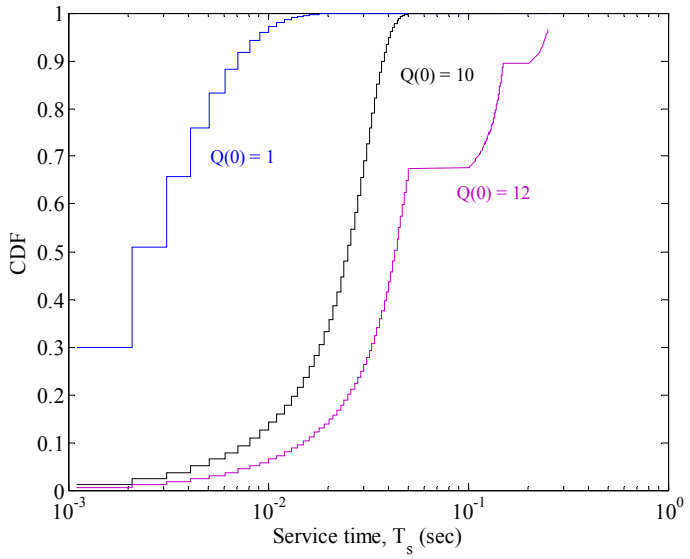

Figure 34. Service time cumulative distribution in linear-log scale. (Probability of transmission in a slot, *p*, is 0.3).

Given the distribution for the service time, we can now use the M/G/1 waiting time equation of (78) to numerically calculate the waiting for slotted ALOHA with periodic server vacations. Substituting this as well as (117) and (118) into (116), we can then solve for the mean total delay of slotted ALOHA with periodic server vacations. This mean total delay is plotted as a function of packet arrival rate in Figure 35 for various values of *K*.

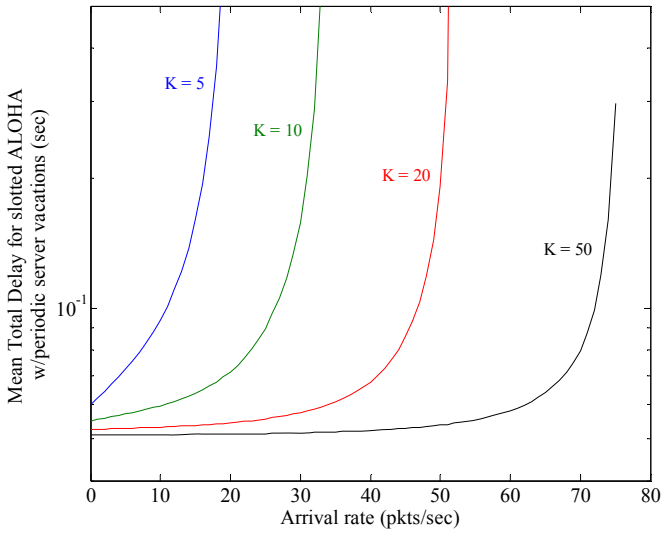

Figure 35. Mean total delay as a function of the packet arrival rate for various numbers of slots in an active period. (Probability of transmission in a slot, *p*, is 0.3).

6. Contention throughput and delay for CWS-MAC

Applying the parameters of CWS MAC from Figure 14 to the throughput and delay results of the previous two sections, the cycle time is equivalent to the slot time t_s, the duration of the active period is *k* minislots of t_{ms} each, and the overhead within an active period is the beacon time t_b. From (115), the normalized mean throughput for the contention mode of CWS-MAC is then

$$S^c = \left(\frac{Q(0) - Q(k)}{t_s} \right) \frac{L_c}{R} \tag{127}$$

where L_c is the contention packet size in bits. The normalized throughput for CWS-MAC is plotted as a function of aggregate contention packet arrival rate in Figure 36 for various values of *k*. Similarly, we can use the results from Section 5 to numerically calculate the mean contention mode delay for CWS-MAC. These results are plotted in Figure 37 again as a function of the aggregate arrival rate for various values of *k*.

We have also plotted the mean residual packets remaining at the end of an active period as well as the contention mode utilization as a function of the aggregate arrival rate in Figures 38 and 39 for various values of *k*. As the utilization approaches one, the mean number of residual packets begin to rise sharply. This is an indication of the saturation of the contention mode.

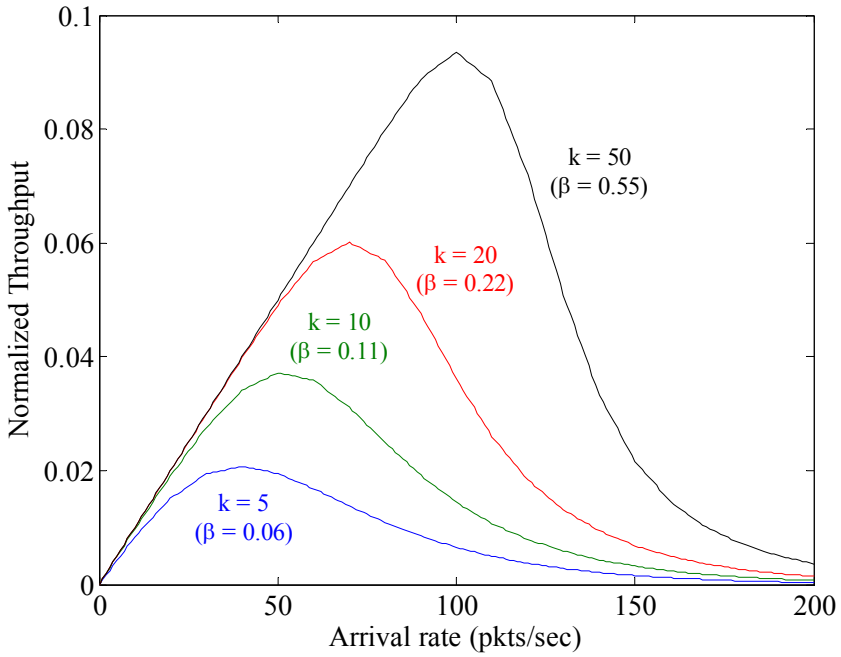

Figure 36. Normalized throughput as a function of the aggregate arrival rate for the contention mode of CWS MAC for various values of *k*. For this plot, the probability of transmission in a slot, *p*, is 0.3.

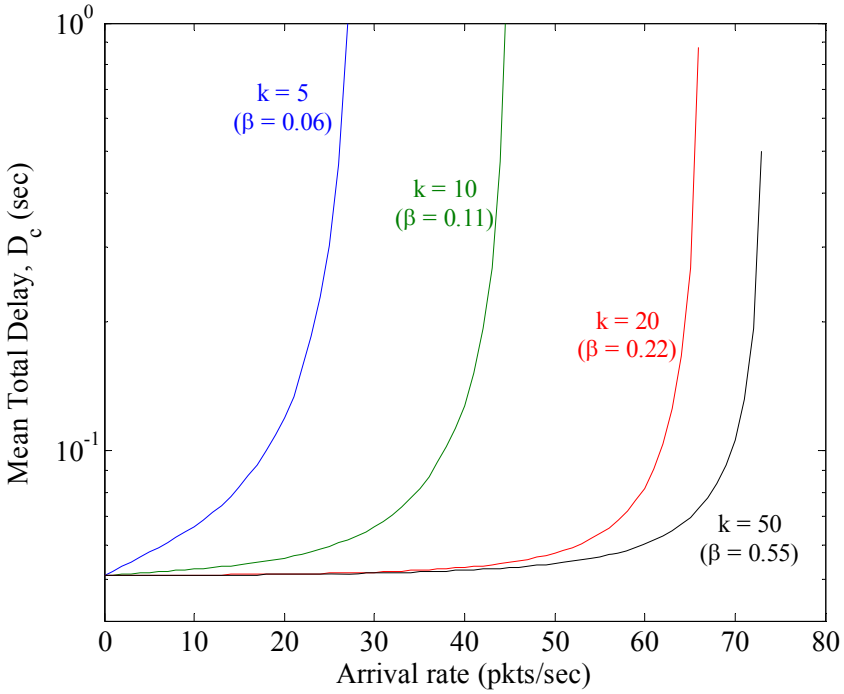

Figure 37. Mean total delay as a function of the aggregate arrival rate for the contention mode of CWS MAC for various values of *k*. For this plot, the probability of transmission in a slot, *p*, is 0.3.

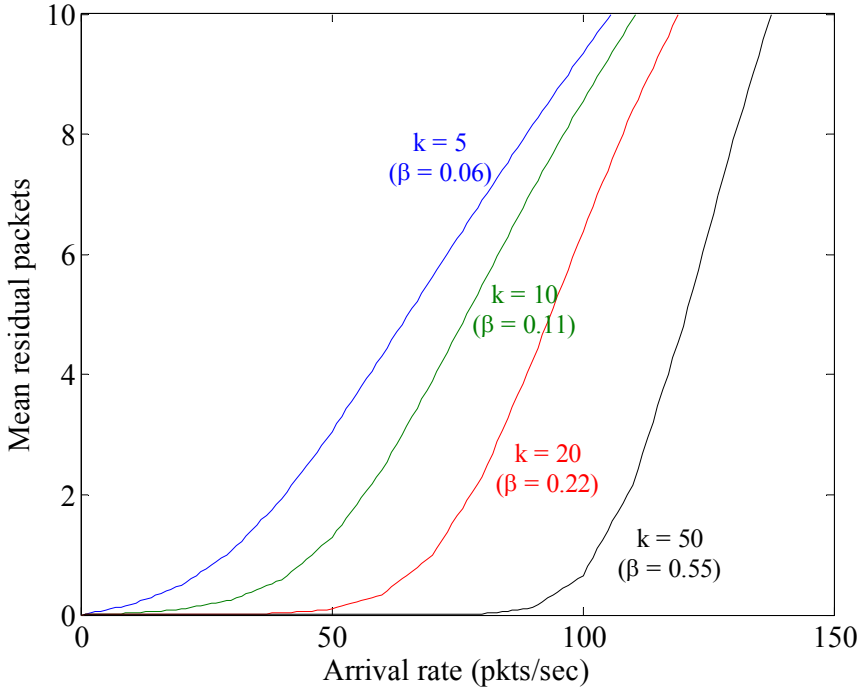

Figure 38. Mean residual packets remaining at the end of the active period as a function of the aggregate arrival rate for the contention mode of CWS MAC for various values of *k*. For this plot, the probability of transmission in a slot, *p*, is 0.3.

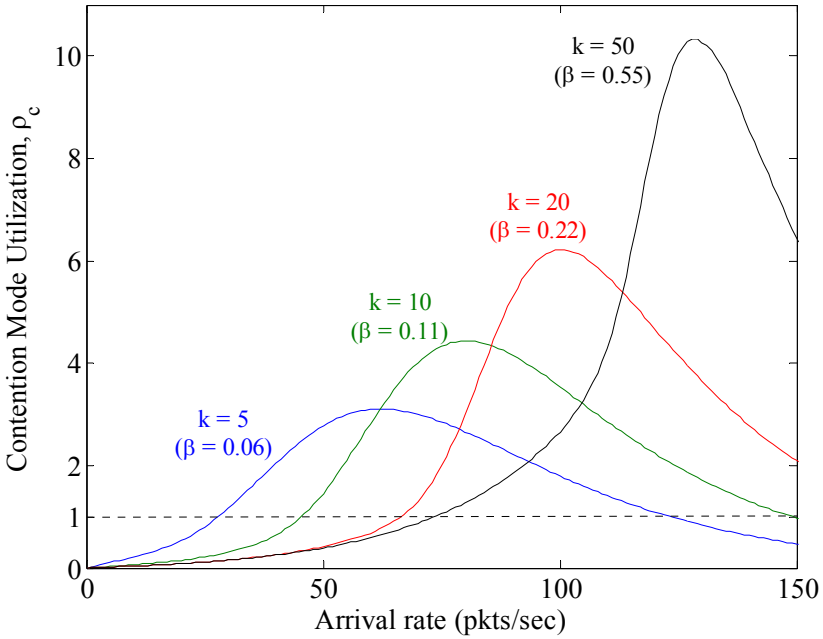

Figure 39. Utilization as a function of the aggregate arrival rate for the contention mode of CWS MAC for various values of *k*. For this plot, the probability of transmission in a slot, *p*, is 0.3.

7. Overall mean delay and throughput for traffic-adaptive CWS-MAC

The results of the previous section can now be applied to the traffic-adaptive model derived in Section III.C for the example of Section II. State 1 of Figure 9 now represents the case where both flows are in the contention mode of traffic-adaptive CWS-MAC while State 2 represents the case where one flow is in the contention mode, but the other has been transitioned to the non-contention mode of traffic-adaptive CWS-MAC. Accordingly, the contention performance parameters S^c and D^c in (15) can be calculated from (115) and the numerical results of Section IV.C.5, respectively, using the combined aggregate flow arrival rate (calculated as the sum of the aggregate arrivals rates for flow 1 and flow 2). Similarly, S_1^c and D_1^c can also be calculated rom (115) and the numerical results of Section IV.C.5, respectively, this time using the arrival rate of flow 1 (assumed to be the flow that is constant and remains in the contention mode). The non-contention performance parameters S_2^{nc} and D_2^{nc} can be calculated from (33) and (100), respectively. The results for the mean total delay for the example of sections II and II.C are plotted in Figures 40 and 41 as function of the combined aggregate packet arrival rate for the various medium access approaches. As expected, traffic-adaptive CWS-MAC outperforms both the contention only and the non-contention only modes as well as the hybrid approach. It can also be seen that, as again expected, the performance of traffic-adaptive CWS-MAC is dependent on the effective choice of the queue-based threshold.

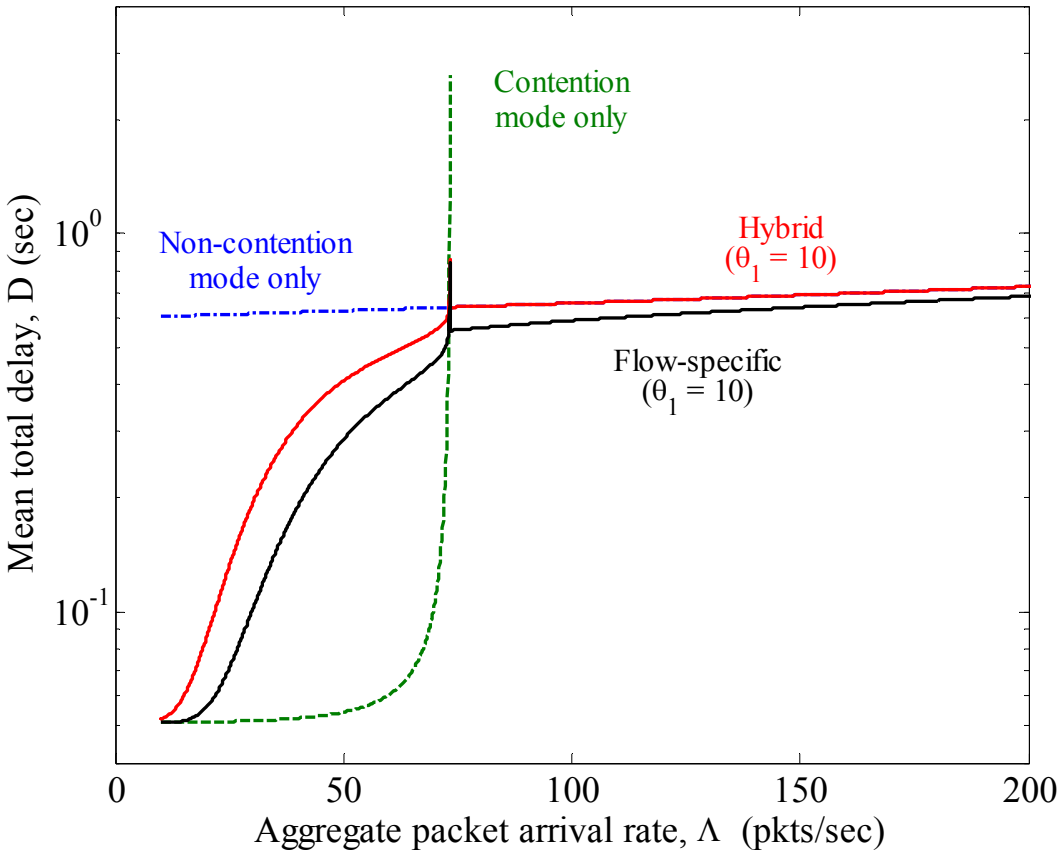

Figure 40. Mean total delay as a function of aggregate arrival rate for contention mode, non-contention mode, hybrid and flow-specific modes for the example of the previous section. For this plot, the probability of transmission in a slot, *p*, is 0.3, channel rate is 1 Mbps, packet size is 1000 bits, and there are 100 slots (one packet length in duration) in the TDMA frame.

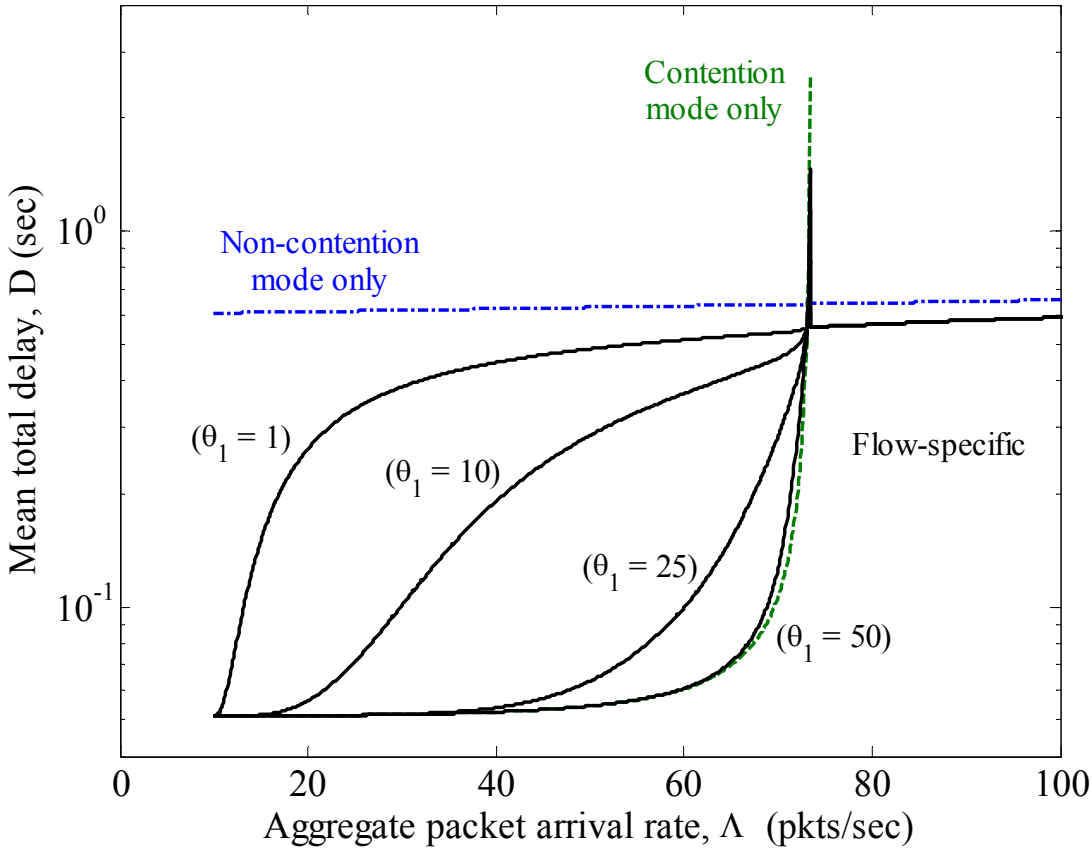

Figure 41. Mean total delay as a function of aggregate arrival rate for various values of θ_1 for flow-specific mode for the example of the previous section. For this plot, the probability of transmission in a slot, *p*, is 0.3, channel rate is 1 Mbps, packet size is 1000 bits, and there are 100 slots (one packet length in duration) in the TDMA frame.

V. SIMULATION RESULTS

In this section, simulation results using the OPNET Modeler suite are provided to demonstrate the effectiveness of the traffic-adaptive, flow-specific scheme. For the simulations, flow 1 load is kept steady at 800 bits/sec (8 packets/sec with a packet size of 100 bits). Flow 2 load is ramped up from zero to a maximum of the channel data rate of 1 Mbps (using a packet size of 1000 bits). Flow 1 represents the fixed rate control flow in the example of Section II, while flow 2 represents the variable data flow. In both cases, the packet size is constant and the packet interarrival times are exponentially distributed. The results were generated with a neighborhood size of 8 nodes where each node is assigned a single slot, a slot size of 0.1 s, a minislot size of 1 ms, a control beacon length of 1 ms, an interframe space of 0.1 ms, and 50 minislots per time slot. The transmission probability in each minislot was chosen as the inverse of the size of the neighborhood. The plotted results are based on Monte Carlo simulations averaged across 100 runs.

End-to end delay and normalized throughput for both flows are presented in Figures 42(a) and 42(b), respectively. With $\theta_1 = 3$ close to optimum, it can be seen that the scheme transitions flow 2 from contention-based to contention-free access as the contention-based mode becomes saturated and the end-to-end packet delay begins to rise. This transition protects the delay bound on flow 1 while providing higher throughput for the heavy load of flow 2. In Figures 43(a) and 43(b), we can compare the performance of different values of θ_1 by taking a closer look at the delay of flow 1 and the throughput of flow 2. For the non-optimum choice of $\theta_1 = 200$, we see that the contention-based mode become saturated prior to transition and the flow 1 delay in Figure 43(a) rises sharply while the flow 2 throughput in Figure 43(b) levels off. Figures 44(a) and 44(b) provide a comparison of the flow-specific end-to-end delay and throughput to that of CSMA and TDMA, respectively. It can be seen that the delay of flow 1 at low loads is better than TDMA while the throughput of flow 2 at high loads is better than CSMA. The CSMA results provided represent best case delay performance as they assume head-of-the-queue privilege for flow 1 and do not include an acknowledgment mechanism.

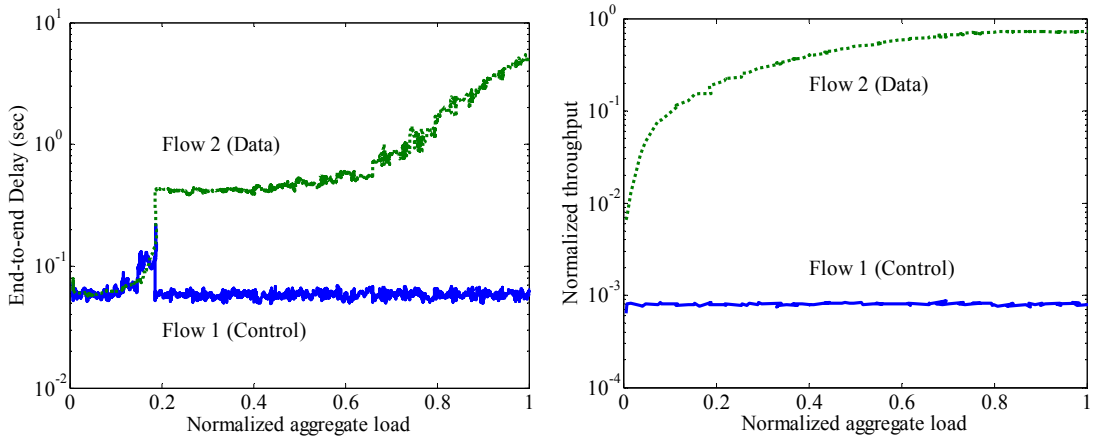

(a) (b)

Figure 42. (a) End-to-end delay and (b) normalized throughput for flow 1 (control) and flow 2 (data) plotted against normalized aggregate load $(\theta_1 = 3)$.

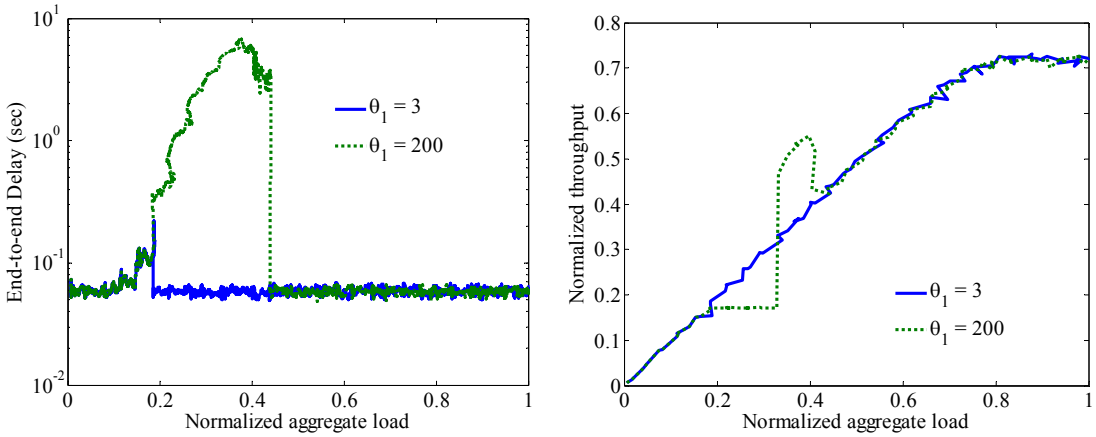

(a) (b)

Figure 43. (a) Flow 1 end-to-end delay plotted as a function of normalized aggregate load for $\theta_1 = 3$ and $\theta_1 = 200$. (b) Flow 2 throughput plotted as a function of normalized aggregate load for $\theta_1 = 3$ and $\theta_1 = 200$.

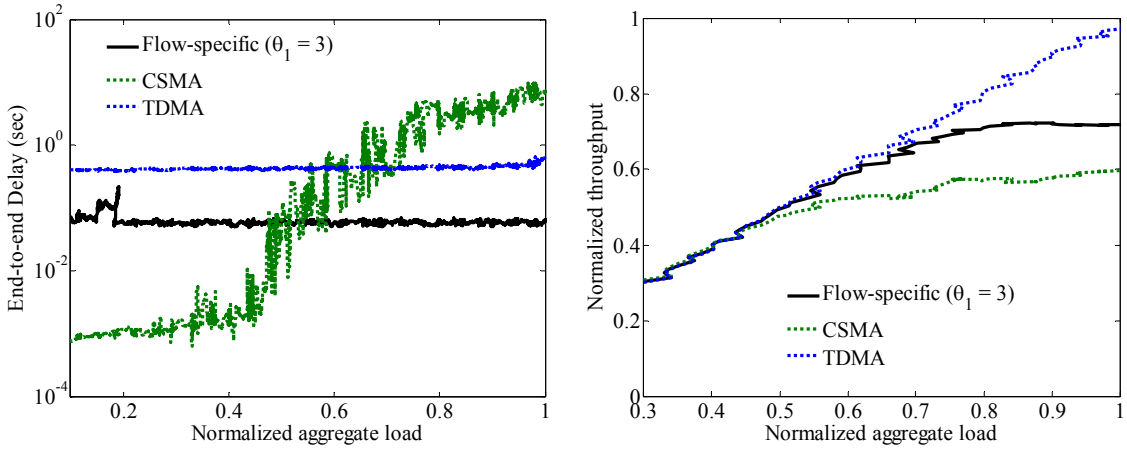

(a) (b)

Figure 44. (a) Flow 1 end-to-end delay and (b) flow 2 throughput compared to CSMA and TDMA for $\theta_1 = 3$.

THIS PAGE INTENTIONALLY LEFT BLANK

VI. CONCLUSIONS

In this report, we formally introduced the concept of traffic-adaptive, flow-specific medium access and showed that, given a suitable switching point, it outperforms traditional contention, non-contention, and hybrid medium access schemes. We proposed a queue-based, traffic-adaptive mechanism and developed a general performance model for traffic-adaptive, flow-specific medium access. We examined the two-flow, two-mode case in detail and also demonstrated that the contention, non-contention, and hybrid approaches are simply special cases of this general medium access model. Finally, we applied the traffic-adaptive mechanism to CWS-MAC, a fixed, flow-specific medium access scheme and provided both performance analysis and simulation results that validated the effectiveness of the traffic-adaptive, flow-specific approach. The performance analysis included delay and throughput analysis for slotted ALOHA with periodic server vacations.

THIS PAGE INTENTIONALLY LEFT BLANK

LIST OF REFERENCES

[1] V. Rajendran, K. Obraczka, and J.J. Garcia-Luna-Aceves, "Energy-efficient, collision-free medium access control for wireless sensor networks," *Wireless. Networks*, vol. 12, no. 1, pp. 63-78, Feb. 2006.

[2] N. Abramson, "The Aloha system - Another alternative for computer communications," *Proc. of the AFIPS Fall Joint Comp. Conf.,* 1970, vol. 37, pp. 281-285.

[3] L. Kleinrock, and F. Tobagi, "Packet switching in radio channels: Part I -Carrier sense multiple-access modes and their throughput-delay characteristics," *IEEE Trans. on Commun.*, vol. 23, no. 12, pp. 1400-1416, Dec. 1975.

[4] I. Rhee, A. Warrier, M. Aia, and J. Min, "Z-MAC: A hybrid MAC for wireless sensor networks," *Proc. of the 3rd Int.l Conf. on Embedded Networked Sensor Systems*, San Diego, California, Nov. 2005, pp. 90-101.

[5] T. O. Walker, M. Tummala, and J. McEachen, "Distributed, flow-based priority medium access control for cooperative multihop wireless Sensor networks," *Proc. of the 41st Ann. Hawaii Intl. Conf. on System Sciences*, Hawaii, Jan. 2008.

[6] L.G. Roberts, "ALOHA packet system with and without slots and capture," *Comp. Commun. Review*, vol. 5, pp. 28-42, Apr. 1975.

[7] S. Lam, "Delay analysis of a time division multiple Access (TDMA) channel," *IEEE Trans. on Commun.*, vol. 25, no. 12, pp. 1489-1494, Dec. 1977.

[8] A. Ephremides, and T. V. Truong, "Scheduling broadcasts in multihop radio networks," *IEEE Trans. on Communications*, vol. 38, no. 4, pp. 456-460, Apr. 1990.

[9] W. Stallings, *High-Speed Networks and Internets: Performance and Quality of Service, Second Edition*. Upper Saddle River, NJ: Prentice Hall, 2002.

[10] S. Floyd and V. Jacobson, "Random early detection gateways for congestion avoidance," *IEEE/ACM Trans. on Networking,* vol. 1, no. 4, pp. 397-413, Aug. 1993.

[11] H. Stark and J. W. Woods, Probability and Random Processes with Applications to Signal Processing (Third Edition). Upper Saddle River, NJ: Prentice Hall, 2002.

[12] R. F. Gebhard, "A queueing process with bilevel hysteretic service-rate control," *Naval Res. Log. Quart.*, vol. 14, pp. 55-68, 1967.

[13] M. Yadin and P. Naor, "On queueing systems with variable service capacities," *Naval Res. Log. Quart.*, vol. 14, pp. 43-54, 1967.

[14] T. O. Walker, M. Tummala, and J. McEachen, "Traffic-adaptive, flow-specific medium access for wireleess networks," Naval Postgraduate School, Monterey, CA, Tech. Rep., in draft.

[15] L. Kleinrock, *Queuing Systems, Volume 1: Theory*, New York: John Wiley & Sons, 1975.

[16] C. Zhu and M. S. Corson, "A five-phase reservation protocol (FPRP) for mobile ad hoc networks," *Proc. of. 17th Ann. Joint Conf. of the IEEE Comp. and Commun. Societies*, Mar. 1998, pp. 322-331.

[17] S. Parthasarathy and R. Gandhi, “Distributed algorithms for coloring and domination in wireless ad hoc networks,” *Proc. Conf. on Foundations of Software Tech. and Theoretical Comp. Science*, Dec 2004, pp. 447-459.

[18] I. Rhee, A. Warrier, J. Min and L. Xu, “DRAND: Distributed randomized TDMA scheduling for wireless ad-hoc networks,” *Proc. of the 7th ACM Intl. Symp. on Mobile Ad Hoc Networking and Computing*, Florence, Italy, May 2006, pp. 190-201.

[19] W. C. Chan, *Performance Analysis of Telecommunications and Local Area Networks*, Boston: Kluwer Academic Publishers, 2000.

[20] L. Kleinrock, and S. S. Lam, "Packet switching in a multi-access broadcast channel: performance evaluation," *IEEE Trans. on Commun.*, vol. 23, no. 4, pp. 410-423, Apr. 1975.

INITIAL DISTRIBUTION LIST

1. Defense Technical Information Center
Ft. Belvoir, Virginia

2. Dudley Knox Library
Naval Postgraduate School
Monterey, California

3. Kirkpatrick, Thomas
SPAWAR SSC ATLANTIC
Charleston, SC

4. Niermann, Michael
SPAWAR SSC ATLANTIC
Charleston, SC

5. Riggins, Michael LCDR
USSOCOM HQ
MacDill AFB, Florida

6. Cathcart, James
National Security Agency
Fort George G. Meade, Maryland

7. Elbert M. Ruiz
National Security Agency
Fort George G. Meade, Maryland

8. John G. Kato
Naval Information Operations Command Suitland
Suitland, Maryland

9. John T. Scott
Naval Information Operations Command Suitland
Suitland, Maryland

10. Murali Tummala
Naval Postgraduate School
Monterey, CA

11. John McEachen
Naval Postgraduate School
Monterey, CA

12. CDR Owens Walker
United States Naval Academy
Annapolis, MD